First Triple-Differential Inclusive ν_μ CC Neutrino Cross Section Measurements from MicroBooNE

London Cooper-Troendle (University of Pittsburgh)

on behalf of the MicroBooNE Collaboration

lcoopert@proton.me

https://arxiv.org/abs/2307.06413

Open Questions in Neutrino Physics

- Is there neutrino sector charge-parity violation?
- Are neutrinos their own anti-particles?
- What is the neutrino mass ordering: $\pm\Delta m^2_{atm}$?
- What are the absolute neutrino masses?
- Are there sterile neutrinos?
- …

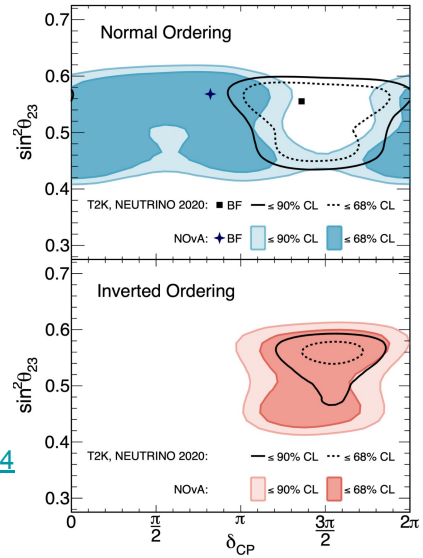

PhysRevD.106.032004

CP Violation Sensitivity

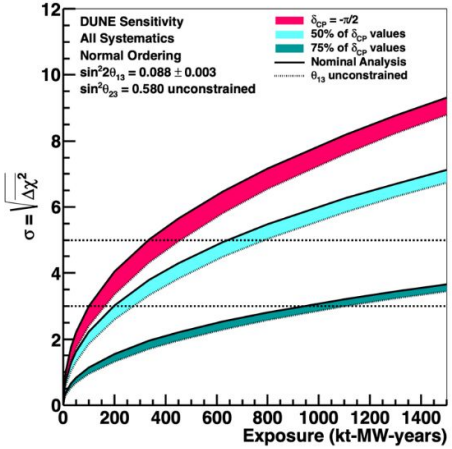

Mass Ordering Sensitivity

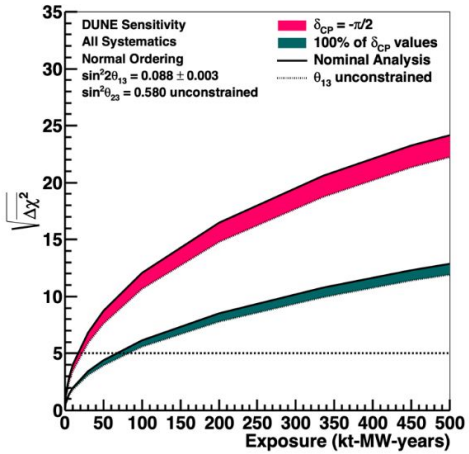

Eur. Phys. J. C (2020) 80:978

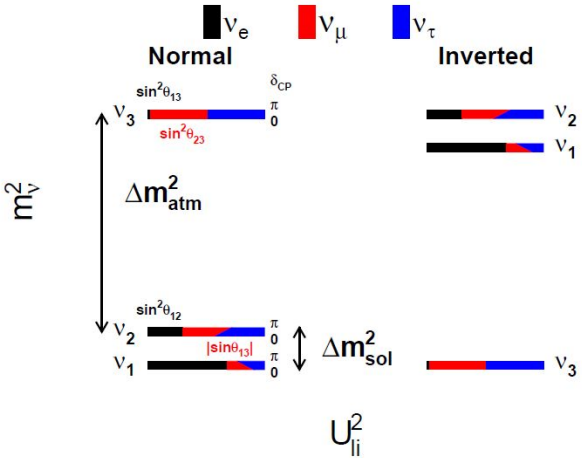

Neutrino Oscillation Experiments

- 30+ experiments over 50 years
- Neutrino oscillations are BSM physics
- Oscillations depend on L/E_ν
  - Don't a priori know E_ν
  - Reconstructing E_ν is critical

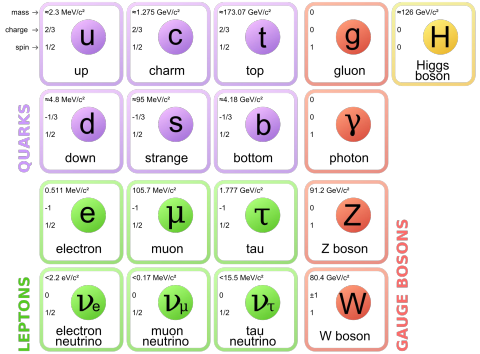

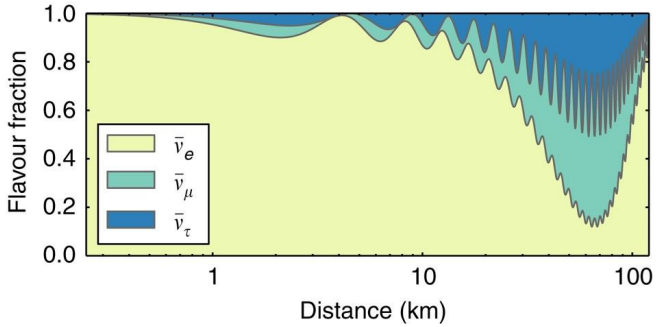

Nature: https://doi.org/10.1038/ncomms7935

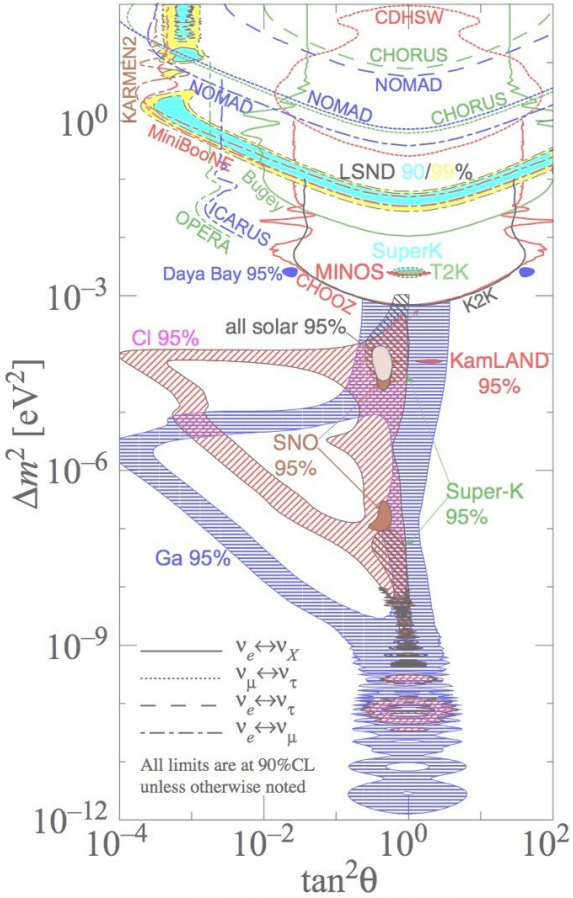

Credit: Hitoshi Murayama

Neutrino Oscillation Experiments

- 30+ experiments over 50 years
- Neutrino oscillations are BSM physics
- Oscillations depend on L/E_ν
  - Don't a priori know E_ν
  - Reconstructing E_ν is critical

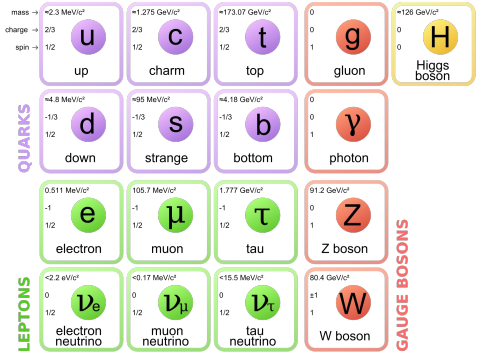

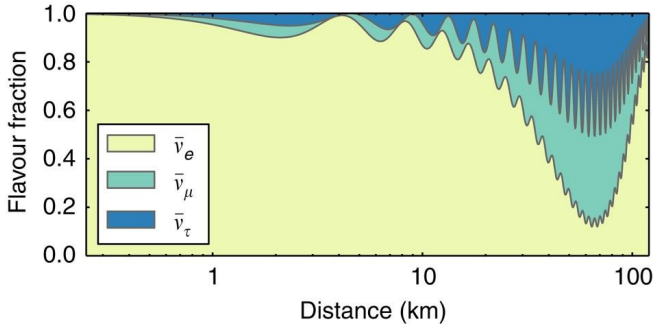

Nature: https://doi.org/10.1038/ncomms7935

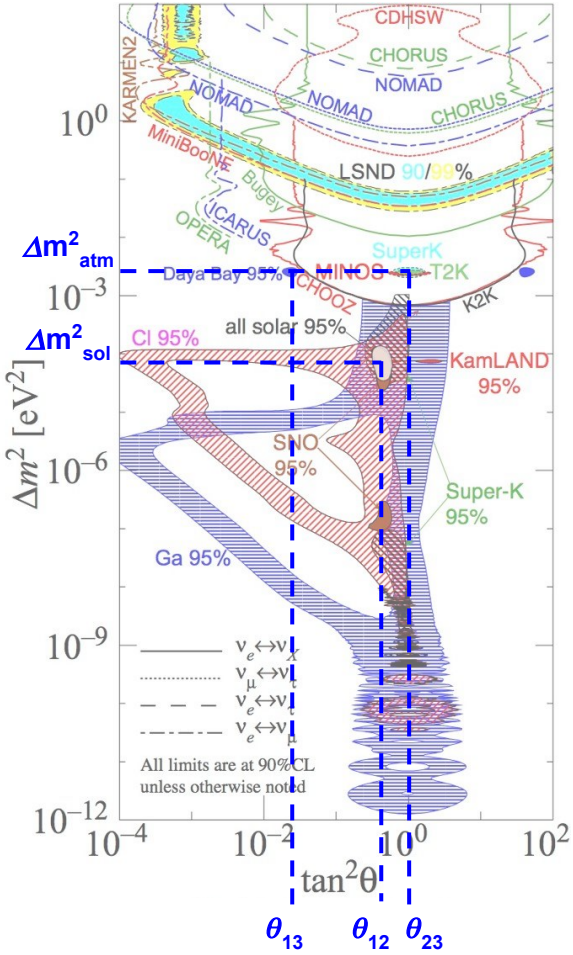

Credit: Hitoshi Murayama

Deep Underground Neutrino Experiment (DUNE)

- Physics goals include: measure δ_{CP} and determine mass ordering
- Far Detector 1300 km away in South Dakota, four 10 kT LArTPCs
- Will measure ν oscillations: ν_e appearance and ν_μ disappearance

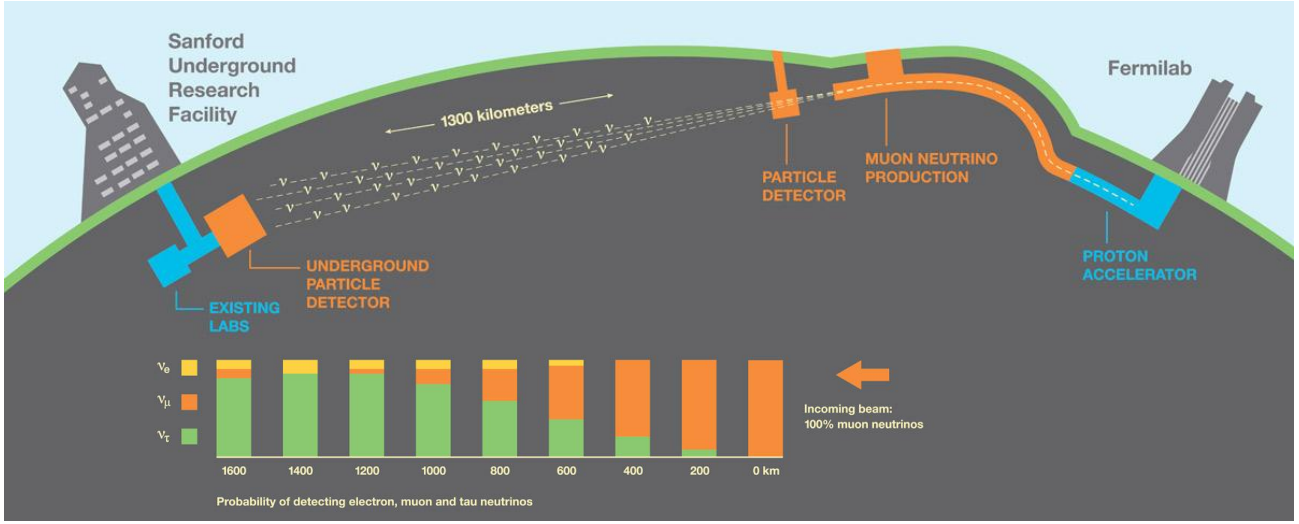

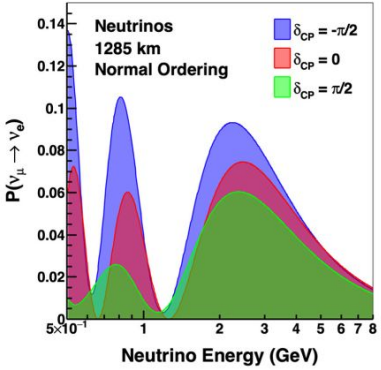

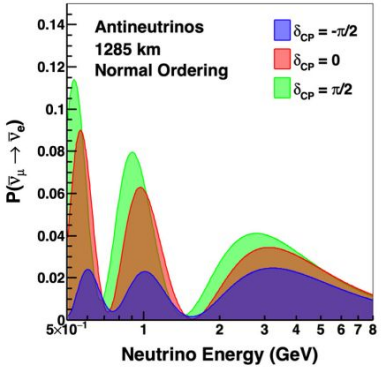

Eur. Phys. J. C (2020) 80:978

Neutrino-Nucleus Interactions

- Future accelerator neutrino experiments require ~GeV energies to determine remaining unknowns
  - Need >105 MeV to produce final state muon
  - MSW “matter effect” is leveraged to determine mass ordering, effect is proportional to E_ν
- (Charged-current) neutrino interactions are complicated and difficult to model in the ~GeV region
- Neutrino interaction modeling plays an important role in oscillation measurements

$$\frac{N_{far}(E_{reco}) = \int P_{\nu\alpha\to\nu\beta}(E_\nu)\cdot\Phi_{far}(E_\nu)\cdot\boldsymbol{\sigma(E_\nu)}\cdot\epsilon(E_\nu)\cdot\mathbf{D(E_\nu\to E_{reco})}\,dE_\nu}{N_{near}(E_{reco}) = \int \Phi_{near}(E_\nu)\cdot\boldsymbol{\sigma(E_\nu)}\cdot\epsilon(E_\nu)\cdot\mathbf{D(E_\nu\to E_{reco})}\,dE_\nu}$$

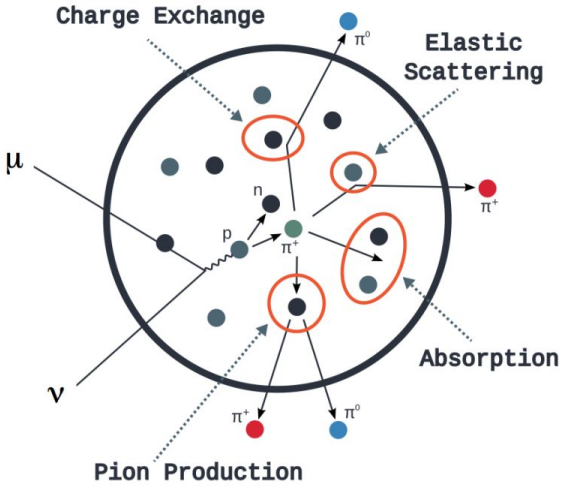

Credit: T. Golan

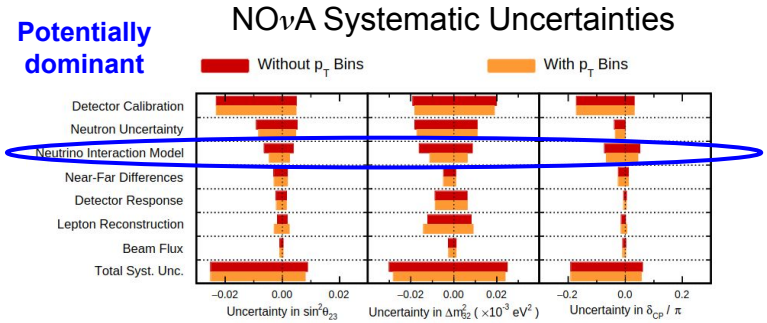

PhysRevD.106.032004

Inclusive ν_μ Charged Current (CC) Interaction Channel

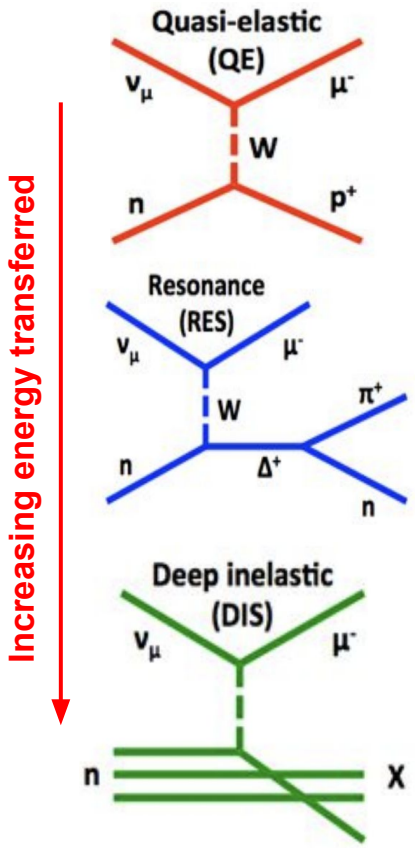

Important to oscillation experiments: outgoing lepton easy to identify

Described by three degrees of freedom ie: $\{E_\nu, P_\mu, \theta_\mu\}$

Particle accelerators produce neutrinos at a range of energies:

- Low energy: **quasi-elastic** interactions scatter off single nucleon
- Intermediate energy: **resonant** interactions excite nucleon
- High energy: **deep inelastic scattering** breaks up nucleon

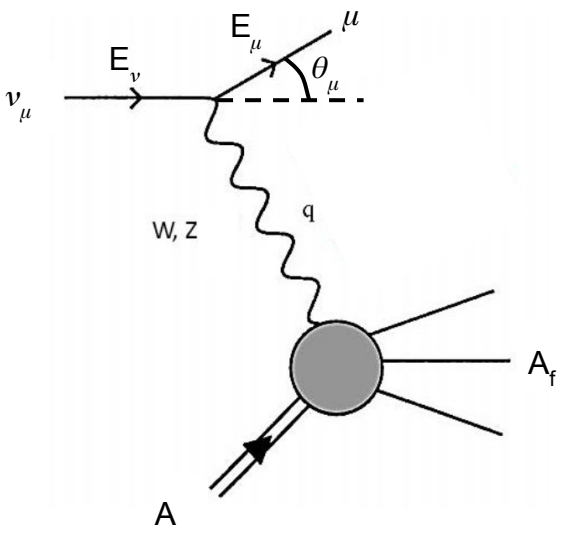

Nuclear Effects

Fermi motion of initial state

- Relativistic Fermi gas, local Fermi gas, correlated Fermi gas
- Spectral functions

Nucleon-nucleon correlations

- Can yield additional final state hadrons, detectable by LArTPC
- 2p2h, meson exchange current (medium range)
- Long range suppressed at low Q^2 (eg: Random Phase Approximation suppression)

Final state interactions (FSI)

- Alter composition and kinematics of particles in the detector
- Impulse approximation
- Intranuclear cascade

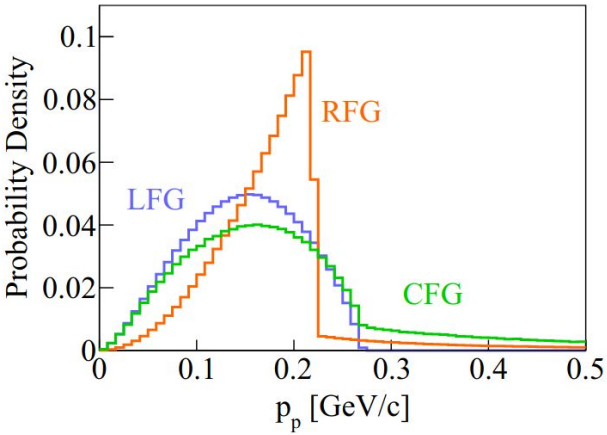

ν_μ CCQE cross section prediction from Genie v3

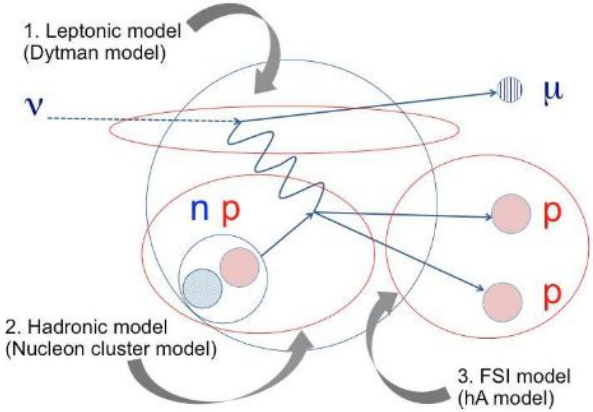

2p2h modeling in Genie v2

Importance of Cross Section Measurements

RevModPhys.84.1307

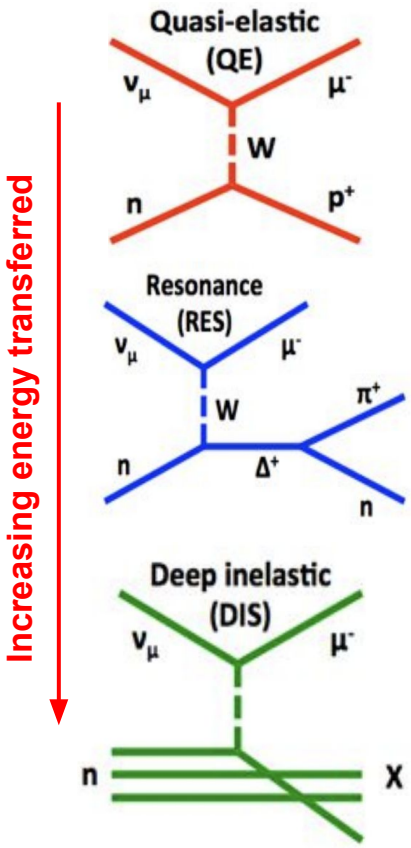

Neutrino interaction modeling is very complicated

- Relies on cross section measurements to guide development

Neutrino experiments rely on models to account for biases:

- Efficiency
- Purity
- Bin migration

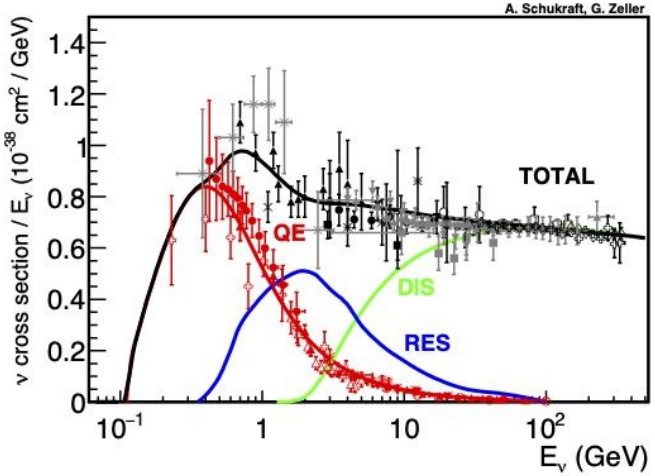

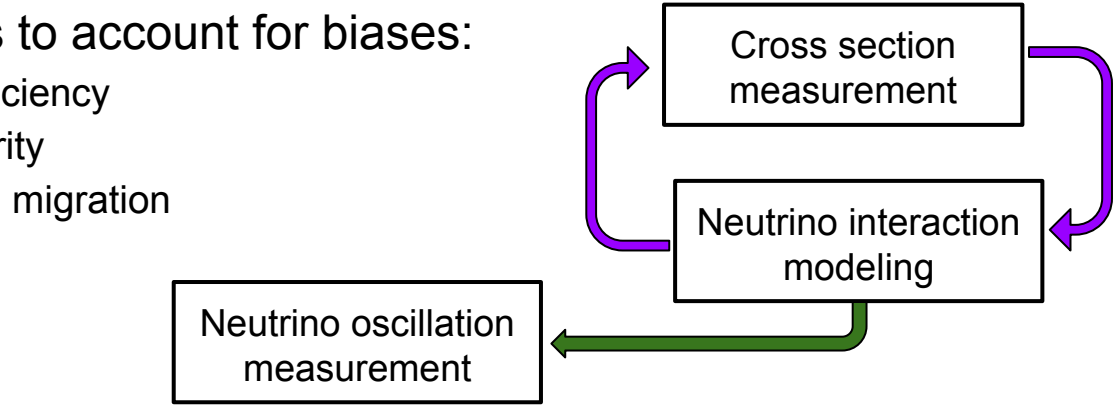

Why we are Interested in E_ν-Dependent Cross Sections

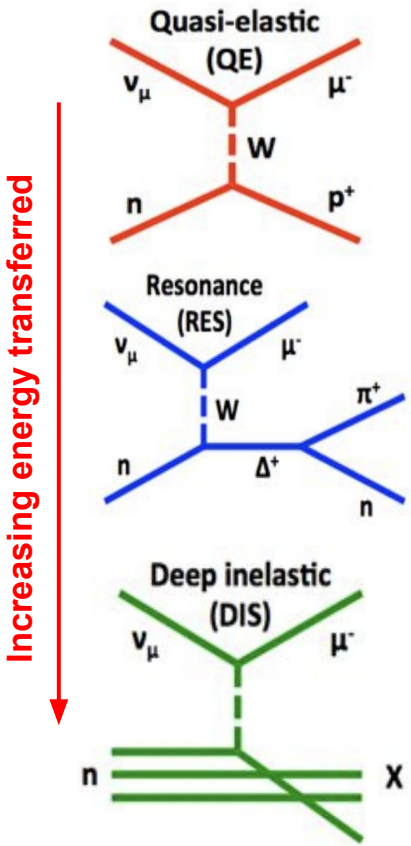

- Oscillations ~ L/E_ν, therefore knowing $\sigma(E_\nu)$ is critical
  - **Wide energy region at DUNE**
- Kinematics of inclusive ν_μCC defined by 3 degrees of freedom, ie: $\{E_\nu, P_\mu, \theta_\mu\}$
  - Triple-differential cross section necessary to span this phase space
  - E_ν is an essential DoF in phase space
  - E_ν can be reconstructed from P_μ and E_{had}

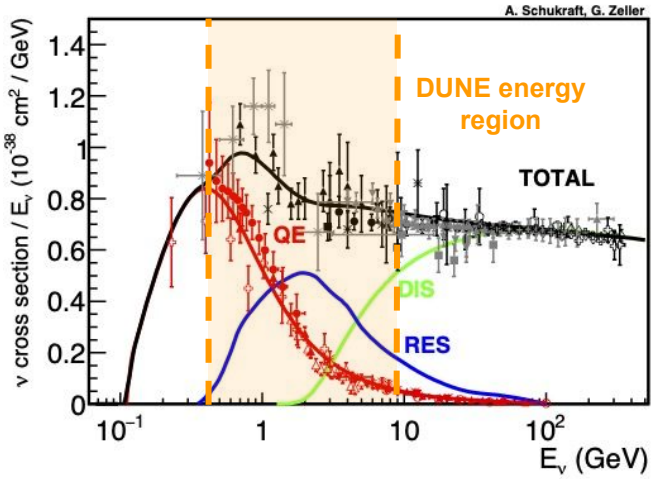

RevModPhys.84.1307

Inclusive ν_μCC in DUNE energy range consists of several major interaction modes (**QE**, **RES**, **DIS**,...)

E_ν-dependent cross sections improve discrimination capabilities

MicroBooNE

Over 150 collaborators from ~40 institutions

60 papers published, with more in the works

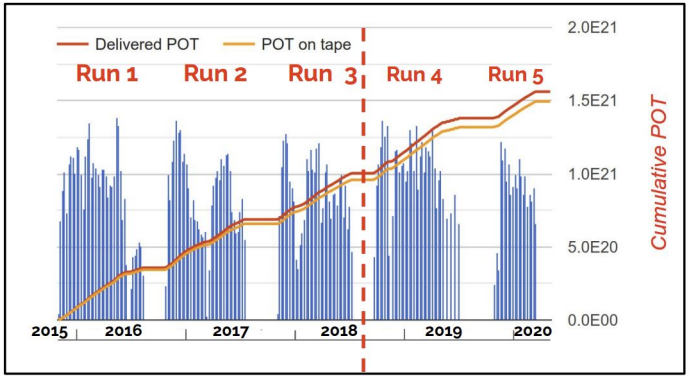

MicroBooNE Papers

2017 2018 2019 2020 2021 2022 2023

First demonstration for a LArTPC-based search for intranuclear neutron-antineutron transitions and annihilation in ^{40}Ar using the MicroBooNE detector
Measurement of triple-differential inclusive muon-neutrino charged-current cross section on argon with the MicroBooNE detector
Measurement of ambient radon daughter decay rates and energy spectra in liquid argon using the MicroBooNE detector
First measurement of η production in neutrino interactions on argon with MicroBooNE
First demonstration of O(1 ns) timing resolution in the MicroBooNE liquid argon time projection chamber
Multi-differential cross section measurements of muon-neutrino-argon quasielastic-like reactions with the MicroBooNE detector
First double-differential measurement of kinematic imbalance in neutrino interactions with the MicroBooNE detector
First measurement of quasi-elastic Λ baryon production in muon antineutrino interactions in the MicroBooNE detector
First measurement of differential cross sections for muon neutrino charged current interactions on argon with a two-proton final state in the MicroBooNE detector
First constraints on light sterile neutrino oscillations from combined appearance and disappearance searches with the MicroBooNE detector
Differential cross section measurements of charged current ν_μ interactions without final-state pions in MicroBooNE
Search for long-lived heavy neutral leptons and Higgs portal scalars decaying in the MicroBooNE detector
Measurement of neutral current single π^0 production on argon with the MicroBooNE detector
Observation of radon mitigation in MicroBooNE by a liquid argon filtration system
Cosmic ray muon clustering for the MicroBooNE liquid argon time projection chamber using sMask-RCNN
Novel approach for evaluating detector-related uncertainties in a LArTPC using MicroBooNE data
First measurement of energy-dependent inclusive muon neutrino charged-current cross sections on argon with the MicroBooNE detector
Search for an anomalous excess of inclusive charged-current ν_e interactions without pions in the final state with the MicroBooNE experiment
Search for an anomalous excess of charged-current quasi-elastic ve interactions with the MicroBooNE experiment using deep-learning-based reconstruction
New theory-driven GENIE tune for MicroBooNE
Search for an anomalous excess of inclusive charged-current ν_e interactions in the MicroBooNE experiment using Wire-Cell reconstruction
Search for an excess of electron neutrino interactions in MicroBooNE using multiple final state topologies
Wire-Cell 3D pattern recognition techniques for neutrino event reconstruction in large LArTPCs
Electromagnetic shower reconstruction and energy validation with Michel electrons and π^0 samples for the deep-learning-based analyses in MicroBooNE
Search for neutrino-induced NC Δ radiative decay in MicroBooNE and a first test of the MiniBooNE low-energy excess under a single-photon hypothesis
First measurement of inclusive electron-neutrino and antineutrino charged current differential cross sections in charged lepton energy on argon in MicroBooNE
Calorimetric classification of track-like signatures in liquid argon TPCs using MicroBooNE data
Search for a Higgs Portal Scalar Decaying to Electron-Positron Pairs in the MicroBooNE Detector
Measurement of the Longitudinal Diffusion of Ionization Electrons in the Detector
Cosmic Ray Background Rejection with Wire-Cell LAr TPC Event Reconstruction in the MicroBooNE Detector
Measurement of the Flux-Averaged Inclusive Charged Current Electron Neutrino and Antineutrino Cross Section on Argon using the NuMI Beam in MicroBooNE
Measurement of the Atmospheric Muon Rate with the MicroBooNE Liquid Argon TPC
Semantic Segmentation with a Sparse Convolutional Neural Network for Event Reconstruction in MicroBooNE
High-performance Generic Neutrino Detection in a LAr TPC near the Earth's Surface with the MicroBooNE Detector
Neutrino Event Selection in the MicroBooNE LAr TPC using Wire-Cell 3D Imaging, Clustering, and Charge-Light Matching
A Convolutional Neural Network for Multiple Particle Identification in the MicroBooNE Liquid Argon Time Projection Chamber
Vertex-Finding and Reconstruction of Contained Two-track Neutrino Events in the MicroBooNE Detector
The Continuous Readout Stream of the MicroBooNE Liquid Argon Time Projection Chamber for Detection of Supernova Burst Neutrinos
Measurement of Differential Cross Sections for Muon Neutrino CC Interactions on Argon with Protons and No Pions in the Final State
Measurement of Space Charge Effects in the MicroBooNE LAr TPC Using Cosmic Muons
First Measurement of Differential Charged Current Quasi-Elastic-Like Muon Neutrino Argon Scattering Cross Sections with the MicroBooNE Detector
Search for heavy neutral leptons decaying into muon-pion pairs in the MicroBooNE detector
Reconstruction and Measurement of O(100) MeV Electromagnetic Activity from Neutral Pion to Gamma Gamma Decays in the MicroBooNE LArTPC
A Method to Determine the Electric Field of Liquid Argon Time Projection Chambers Using a UV Laser System and its Application in MicroBooNE
Calibration of the Charge and Energy Response of the MicroBooNE Liquid Argon Time Projection Chamber Using Muons and Protons
First Measurement of Inclusive Muon Neutrino Charged Current Differential Cross Sections on Argon at Enu ~0.8 GeV with the MicroBooNE Detector
Design and Construction of the MicroBooNE Cosmic Ray Tagger System
Rejecting Cosmic Background for Exclusive Neutrino Interaction Studies with Liquid Argon TPCs: A Case Study with the MicroBooNE Detector
First Measurement of Muon Neutrino Charged Current Neutral Pion Production on Argon with the MicroBooNE detector
A Deep Neural Network for Pixel-Level Electromagnetic Particle Identification in the MicroBooNE Liquid Argon Time Projection Chamber
Comparison of Muon-Neutrino-Argon Multiplicity Distributions Observed by MicroBooNE to GENIE Model Predictions
Ionization Electron Signal Processing in Single Phase LArTPCs II: Data/Simulation Comparison and Performance in MicroBooNE
Ionization Electron Signal Processing in Single Phase LArTPCs I: Algorithm Description and Quantitative Evaluation with MicroBooNE Simulation
The Pandora Multi-Algorithm Approach to Automated Pattern Recognition of Cosmic Ray Muon and Neutrino Events in the MicroBooNE Detector
Measurement of Cosmic Ray Reconstruction Efficiencies in the MicroBooNE LAr TPC Using a Small External Cosmic Ray Counter
Noise Characterization and Filtering in the MicroBooNE Liquid Argon TPC
Michel Electron Reconstruction Using Cosmic Ray Data from the MicroBooNE LAr TPC
Determination of Muon Momentum in the MicroBooNE LAr TPC Using an Improved Model of Multiple Coulomb Scattering
Convolutional Neural Networks Applied to Neutrino Events in a Liquid Argon Time Projection Chamber
Design and Construction of the MicroBooNE Detector

The Booster Neutrino Beam

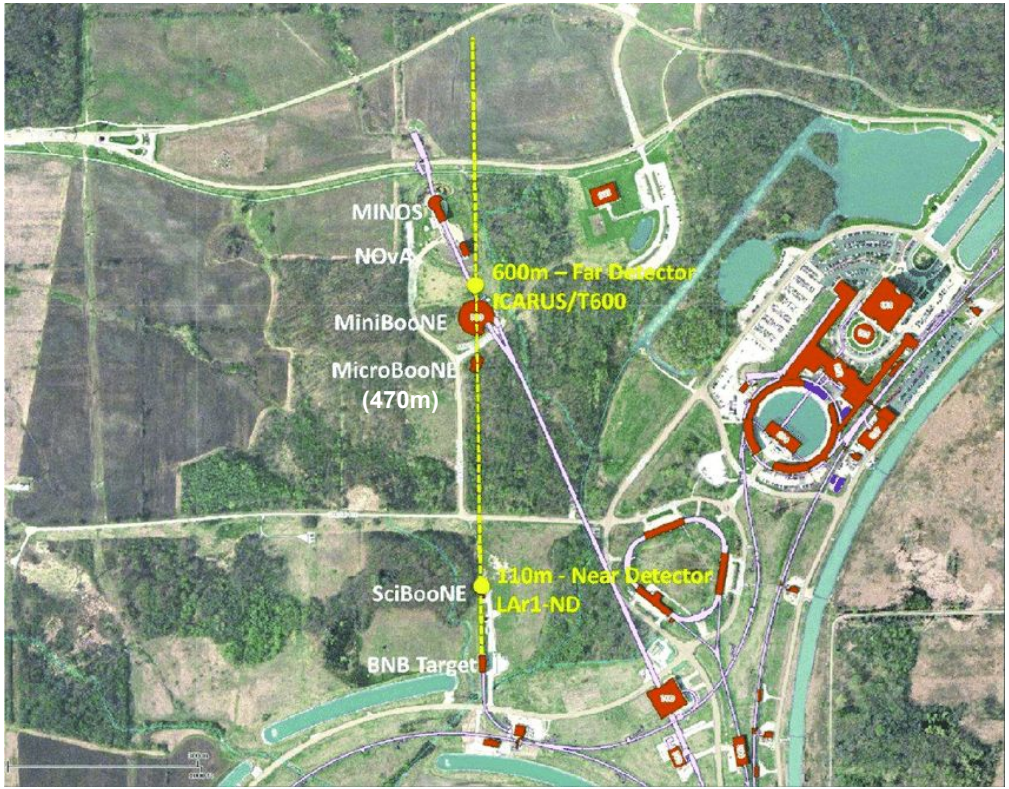

Fermilab campus

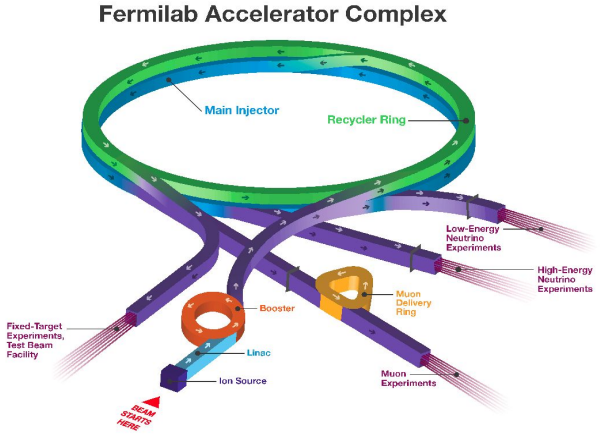

Neutrino flux at MicroBooNE detector location

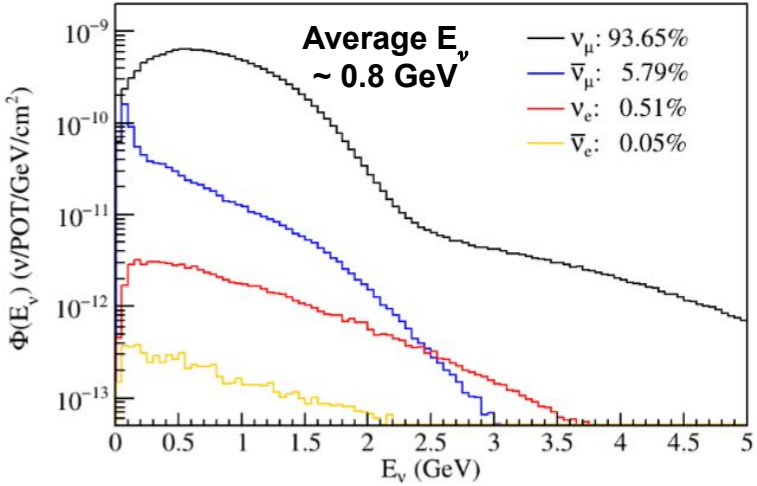

Liquid Argon Time Projection Chamber (LArTPC)

The MicroBooNE detector is an 85-tonne LArTPC

- Fully active
- ~mm level position reconstruction
- Calorimetry for energy reconstruction and particle identification
- 32 Photomultiplier tubes (PMTs) capture prompt scintillation light

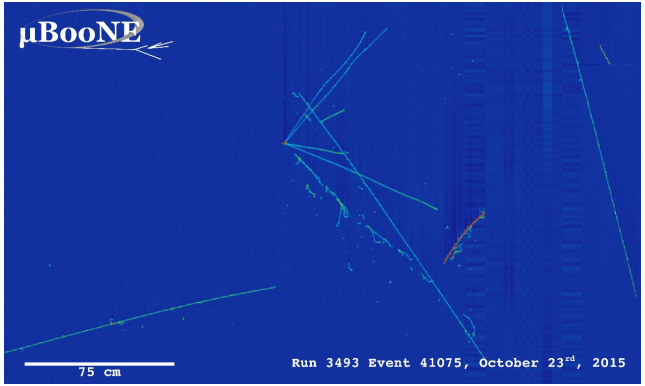

Detector

Wire Planes

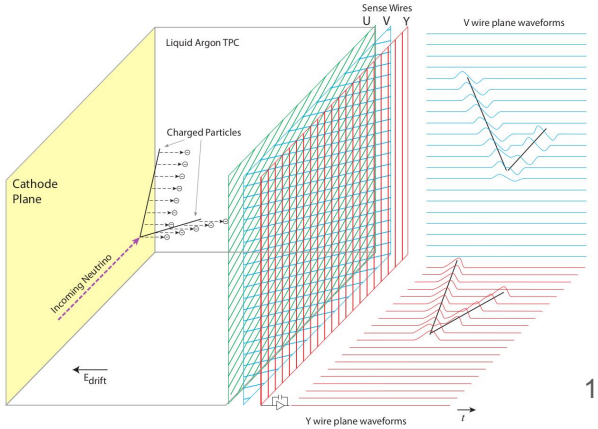

Cross Section Measurements at MicroBooNE and Beyond

Inclusive ν_μ CC Double-Differential Cross Section

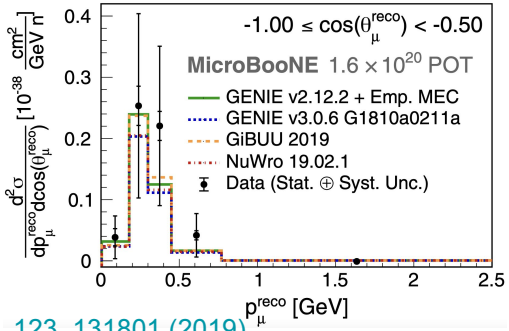

PRL 123, 131801 (2019)

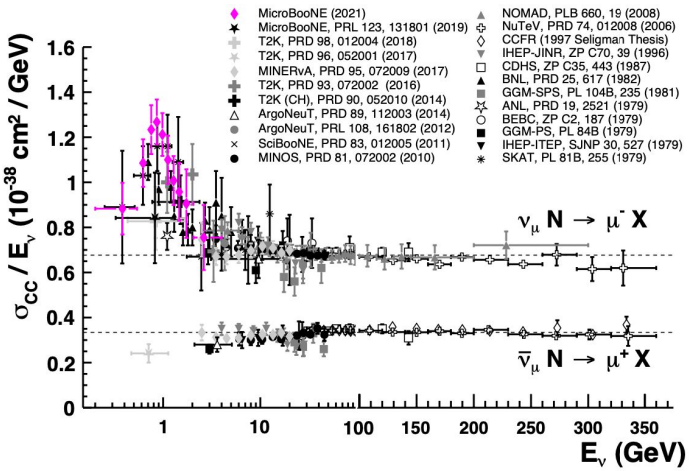

Other results from MicroBooNE:

PhysRevLett.128.151801(2022)
PRD 104, 052002 (2021)
PRL 125, 201803 (2020)
PRD 102, 112013 (2020)
PRD 99, 091102 (2019)

And more!

ν_μ CC 1p0pi Kinematic Imbalance Double-Differential Cross Section

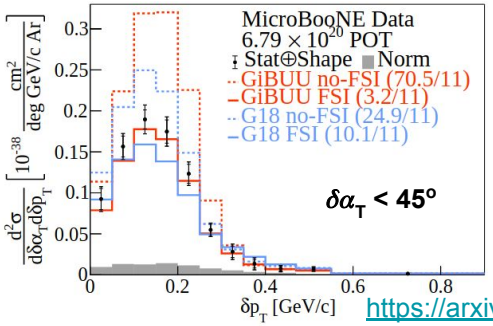

https://arxiv.org/abs/2301.03706

Inclusive ν_μ CC Measurements

Experiment	Target	References	Efficiency (%)	Purity (%)
ArgoNeuT	Ar	Phys. Rev. Lett. 108 161802 Phys. Rev. D 89 112003	49.5 42.0 (59.0)	95 95.2 (91.2)
MicroBooNE	Ar	Phys. Rev. Lett. 123 131801 Phys. Rev. Lett. **128**, 151801	57.2 68	50.4 92
MINERvA	CH, C/CH, Fe/CH, Pb/CH	Phys. Rev. Lett. 112, 231801 Phys. Rev. D94, 112007 Phys. Rev. Lett. 116	24 ~ 50	60 ~ 80
MINOS	Fe	Phys. Rev. D81, 072002		
NOMAD	C	Phys. Lett. B660, 19	40.9 ~ 73.3	99.3
SciBooNE	CH	Phys. Rev. D83, 12005	34.5	~90
T2K	CH, H_2O, Fe	Phys. Rev. D87, 092003 Phys. Rev. D90, 052010 Phys. Rev. D93, 072002	~50 41.2 ~50 @1GeV	~86 89.4 ~97

Wire Cell Reconstruction

- One of three reconstruction paradigms at MicroBooNE
- Resourcefully leverages detector information to produce high quality reconstruction
- Has helped produce great physics results at MicroBooNE

MicroBooNE Low Energy Excess: PhysRevD.105.112005

MicroBooNE Sterile Neutrino Search: PhysRevLett.130.011801

JINST 13 P07006

Signal Processing

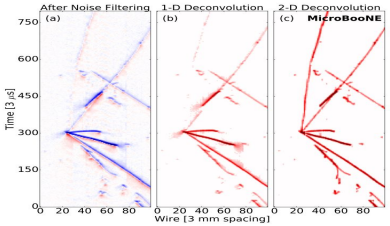

JINST 16 P06043

Imaging

Clustering

Matching

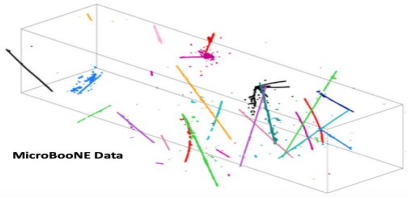

PhysRevApplied.15.064071

Trajectory and dQ/dx Fit

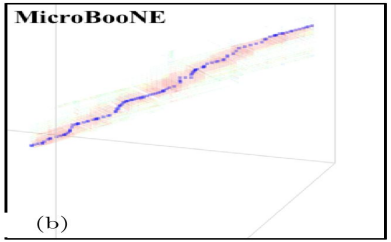

JINST 17 P01037

Pattern Recognition:

PID and Vertexing

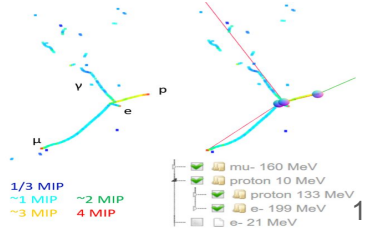

Charge-Light Matching

- MicroBooNE surface location + slow LArTPC detector (2,300 μs readout) = huge cosmic ray background
  - 1.6 μs beam window can reject overwhelming majority
  - Light info is prompt, timing at ~ns level
  - Charge-light matching connects light info to charge cluster

- Many-to-many matching: attempt to match every flash and cluster
  - Reduces neutrino flash mismatch error rate, **improving selection purity**
  - Determining cosmic ray timing enables a suite of background removal algorithms, **improving efficiency** and purity
  - Allows the inclusion of partially contained (PC) events, tripling statistics; particularly beneficial at high energy

MicroBooNE Data

JINST 16 P06043

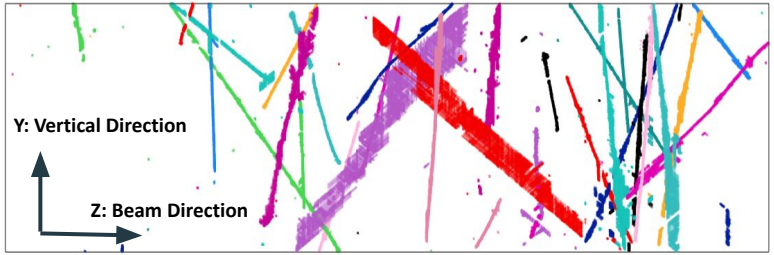

Top: a drift window with ~20 cosmic rays

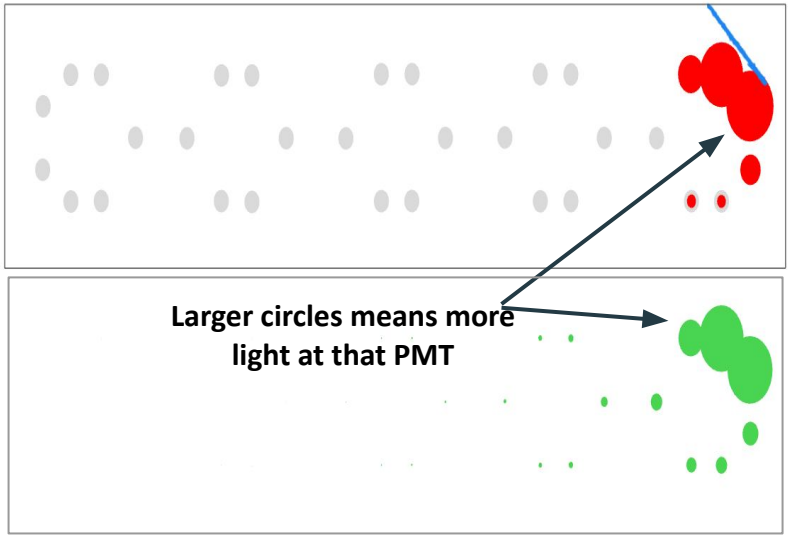

Bottom: The observed (upper) and predicted (lower) light patterns for a single cosmic ray.

ν_μ CC Selection

- Large dataset to enable cross section measurements
  - 6.4 x 10^{20} POT
  - ~110k ν_μ CC events
  - Sufficient for multi-differential cross section measurements
- Non-zero selection efficiency across phase space
  - Enabled by high-quality event reconstruction
  - Necessary for reliable model validation

Selection Cut	Efficiency	Purity
Hardware Trigger	1	5×10^{-5}
Software Trigger	98%	5×10^{-3}
Charge-Light Matching	92%	11%
Generic Neutrino Selection	80%	65%
ν_μ CC Selection	**68%**	**92%**

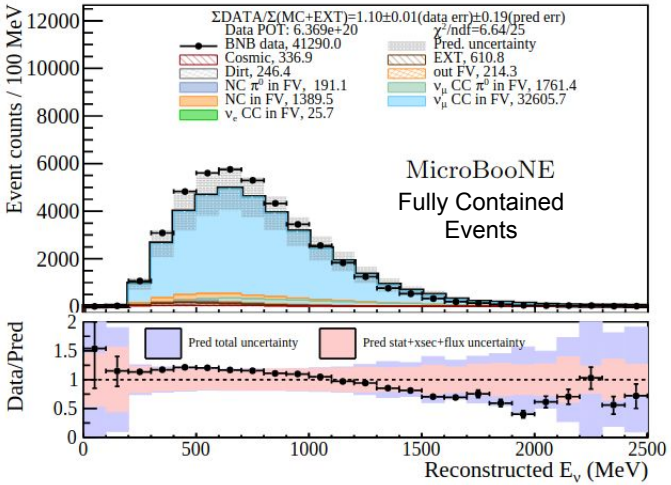

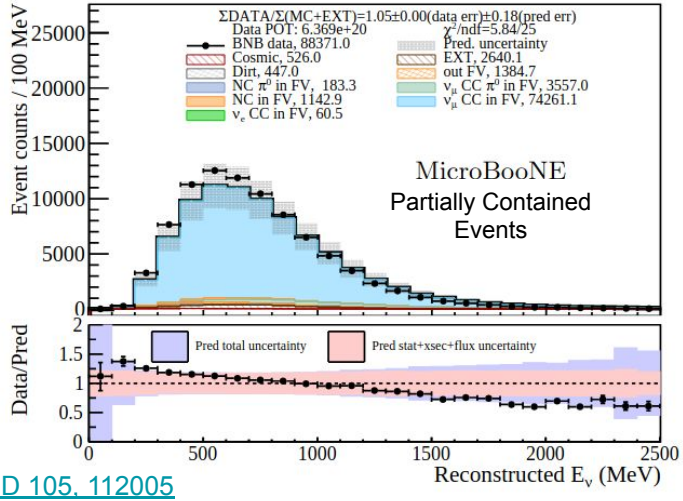

Phys. Rev. D 105, 112005

Neutrino Energy Reconstruction

- $E_\nu = \Sigma E_{particle}$
  - Mass included for muons and pions
  - 8.6 MeV binding energy included per proton
- Tracks:
  - Residual range → energy is default, summed dE/dx in edge cases
  - Calibrated using stopped muons and protons
- Showers:
  - Scaled charge to account for recombination and bias
  - Calibrated using π^0 mass reconstruction
- Fully Contained (FC) E_ν^{rec} resolution: 15-20%

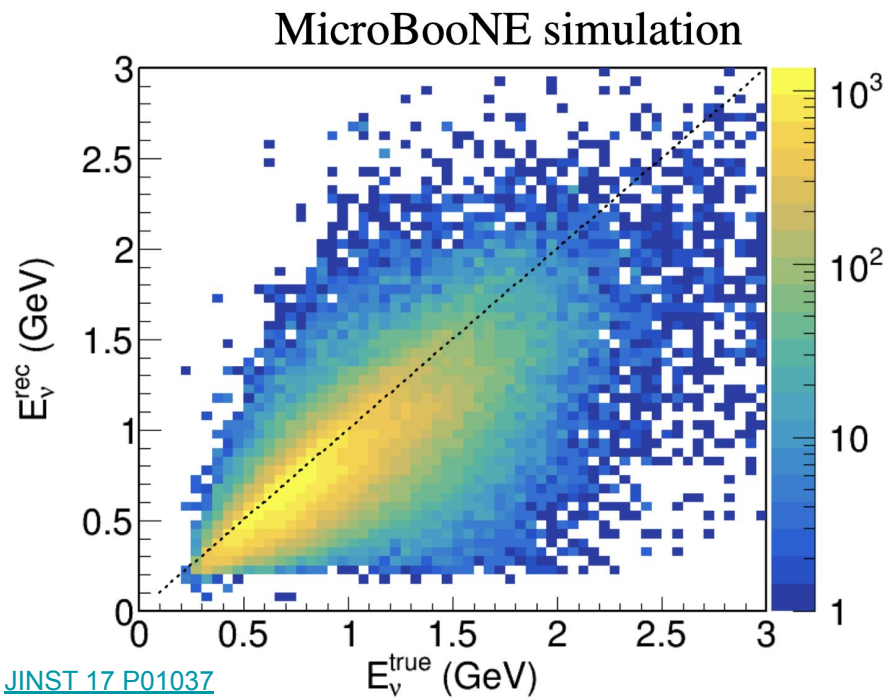

JINST 17 P01037

Neutrino energy resolution for fully contained charged current events

Choice of Binning in 3D

- Binning chosen to respect detector resolutions
  - 15-20% in E_ν
  - 10-15% in P_μ
  - Up to 5° in θ_μ at forward angles
- 4 E_ν slices
  - Edges: {0.2, 0.705, 1.05, 1.57, 4} GeV
- 9 $\cos(\theta_\mu)$ slices
  - Edges: {−1,−0.5, 0, 0.27, 0.45, 0.62, 0.76, 0.86, 0.94, 1}
- 3-6 P_μ bins per slice
  - Edges: {0, 0.18, 0.3, 0.45, 0.61, 0.77, 0.97, 1.28, 1.66, 2.5} GeV/c
- 138 Analysis bins in total

Binning for E_ν in [0.2,0.705] GeV

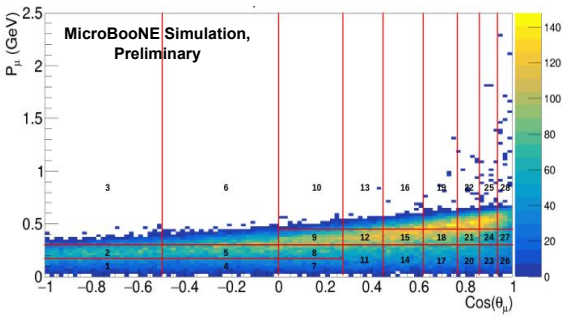

Binning for E_ν in [0.705,1.05] GeV

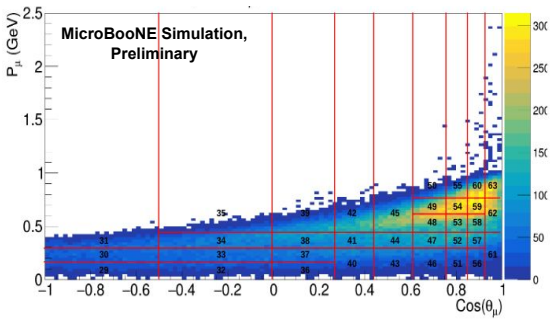

Binning for E_ν in [1.05,1.57] GeV

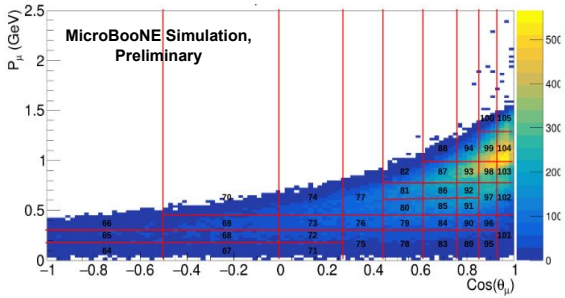

Binning for E_ν in [1.57,4.0] GeV

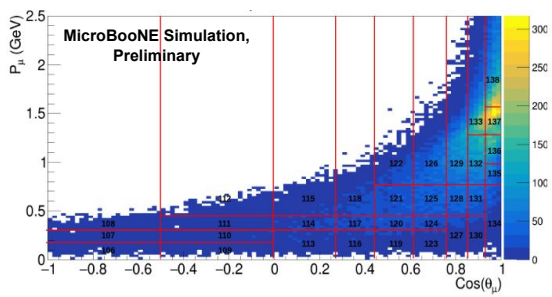

Selection Efficiency in 3D

Pixels with low MC sample size not drawn

Bins consist of multiple pixels so that sample size per bin is sufficient

- Estimated using MC simulation
  - Selection rate shown for events with truth values in given pixel
- Non-zero efficiency across full phase space
  - Necessary for data-driven model validation - can't validate regions without data

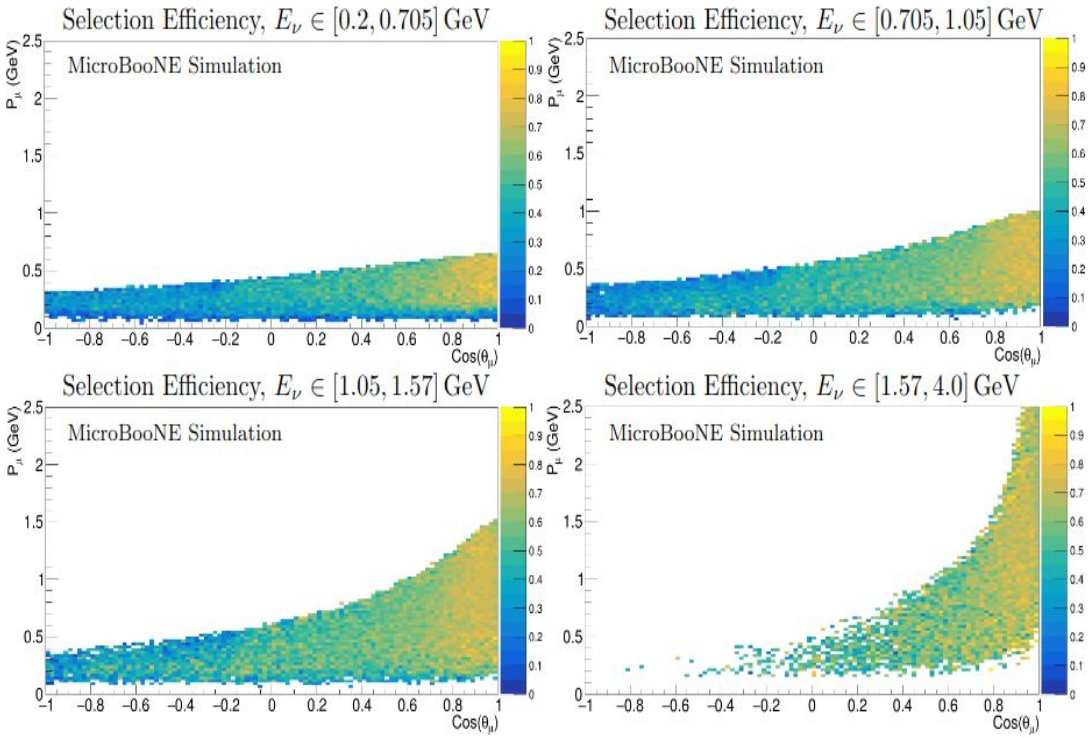

https://arxiv.org/abs/2307.06413

Event Generator Details

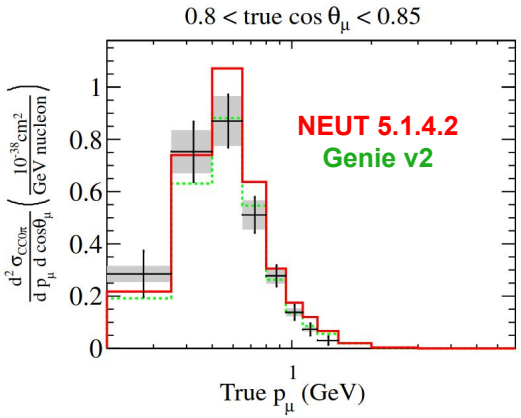

MicroBooNE model uses Genie v3.0.6 G18_10a_02_11a tuned to T2k data (right, Phys Rev D. 93, 112012)

Local Fermi Gas (LFG):

- Nuclear initial state is degenerate gas up to Fermi momentum $p_F(r)$

Valencia model includes random phase approximation:

- Description of long-range n-n correlations via effective potential

FSI modeled using hA:

- Approximates numerous hadron-nucleus interactions with a total cross section

	Genie 3.0.6	NEUT 5.4.0.1	NuWRo 19.2.1	GiBUU 2021
Nuclear Model	**LFG**	**LFG**	**LFG**	**LFG**
QE	**Valencia**	**Nieves**	**Lwlyn-Smith**	**standard**
MEC	**Valencia**	**Nieves**	**Nieves**	**empirical**
Resonant	**KLN-BS**	**Berger-Sehgal**	**Adler-Rarita-Schwinger**	**MAID (Spin-dependent)**
Coherent	**Berger-Sehgal**	**Rein-Sehgal**	**Berger-Sehgal**	
FSI	**hA2018 cascade**	**cascade**	**cascade**	**BUU transport model**

Systematic Uncertainties

- **MC statistical uncertainty**: estimated with Poisson likelihood with a Bayesian approach
- **Flux prediction**: MiniBooNE prediction updated to MicroBooNE baseline
  - PRD 79, 072002
- **Cross Section (XS)**: Modeled using Genie v3.0.6 G18_10a_02_11a tuned to T2K CC0π data
  - PRD 105, 072001, Eur. Phys. J. Spec. Top. 230, 4449–4467 (2021)
- **Detector Response**: TPC waveform, light yield, space charge effect, recombination
  - Estimated using bootstrapping (event resampling)
  - Many bins in 3D + limited MC events → statistical fluctuations →overestimate uncertainty

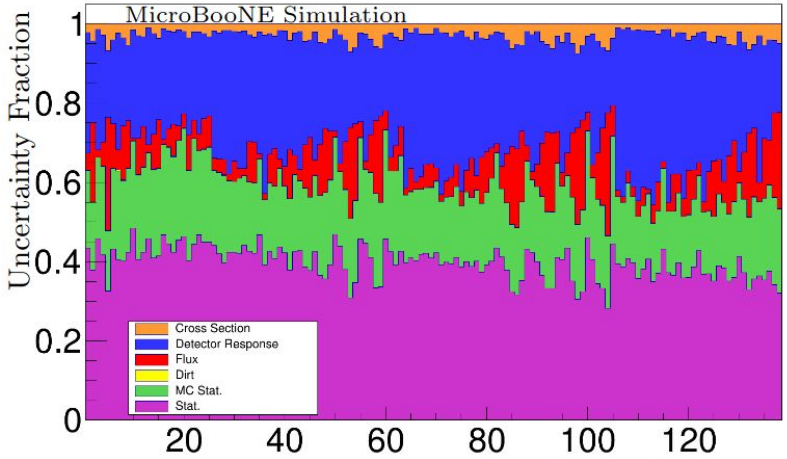

Breakdown of uncertainties fraction across 138 analysis bins

https://arxiv.org/abs/2307.06413

Additional (smaller) uncertainties:

- ν interaction outside cryostat
- GEANT4 model reweighting
- POT from originating proton flux
- Number of target nuclei

Gaussian Processes Smoothing

- Many bins in 3D + limited MC events →statistical fluctuations →overestimate uncertainty
- Gaussian processes asserts smoothness intuition that nearby bins are correlated
- Smoothed uncertainties consistent with increased statistics in 1D test

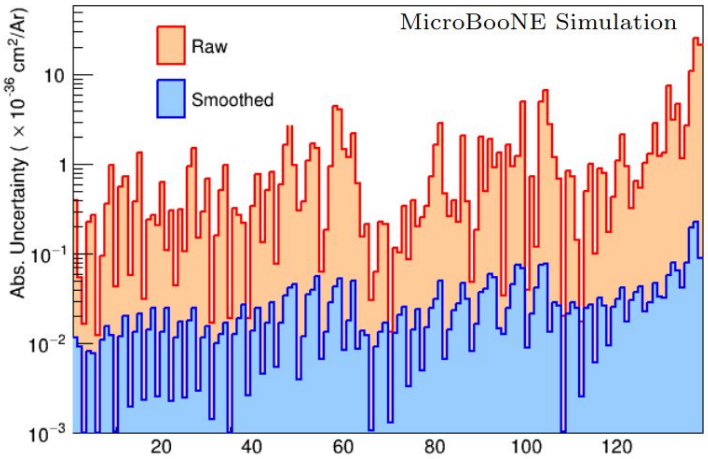

Detector response uncertainties **with** and **without** smoothing

https://arxiv.org/abs/2307.06413

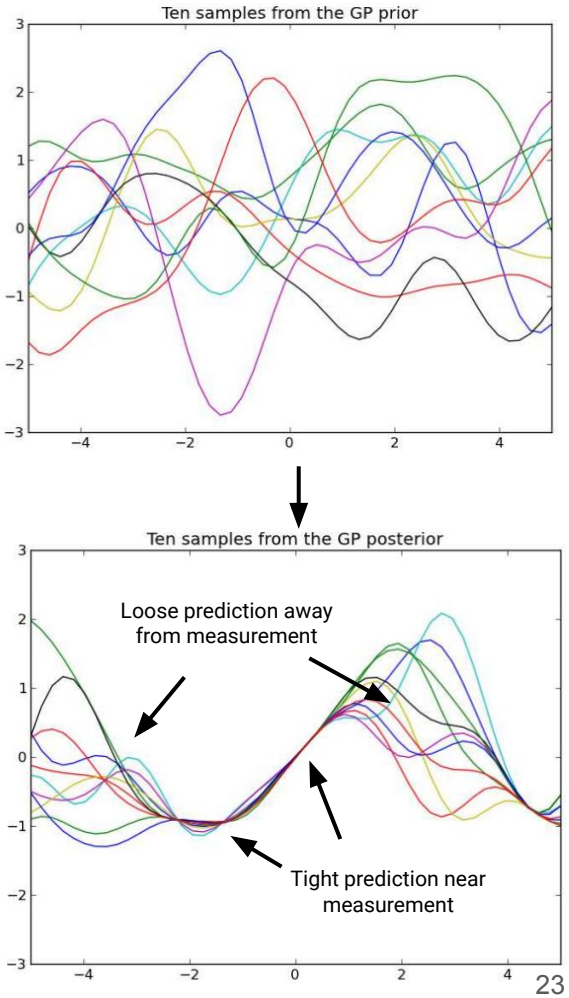

Importance of Model Validation

A neutrino flux model is required to compare **any** neutrino cross section measurement to a theoretical or event generator prediction

Model validation lets us understand the level of potential model bias we introduce

1. Validate modeling of missing hadronic energy
   a. Novel validation test using conditional constraint
   b. Allows confident unfolding to true E_ν
2. Unfold and present results

Model Validation: $M(E_{had}^{vis})$ vs $\mu(E_{had}^{vis}|E_\nu, E_\mu^{reco})$

Given by neutrino flux modeling

Muon kinematics measurement

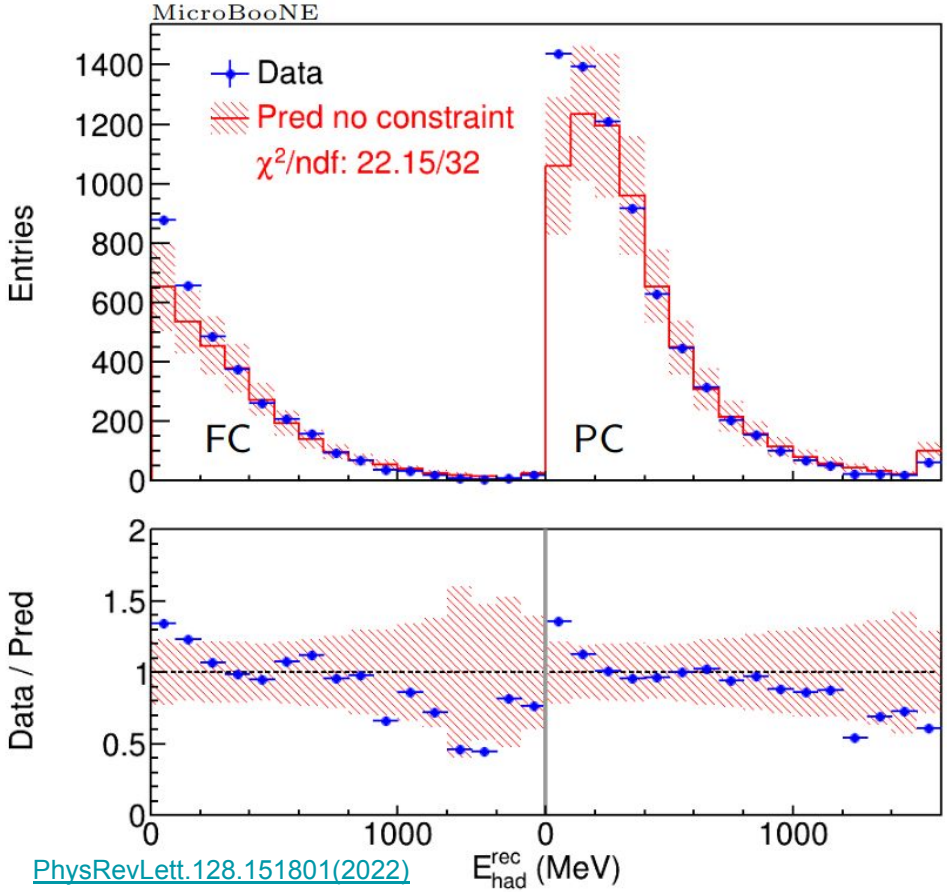

PhysRevLett.128.151801(2022)

- New method to validate the modeling of neutrino energy
  - Uses LArTPC measurements of lepton kinematics and hadronic energy
- Data/MC goodness of fit tested with χ^2/ndf
  - Muon kinematics used to constrain model prediction of hadronic energy under conditional constraint formalism

Model Validation: $M(E_{had}^{vis})$ vs $\mu(E_{had}^{vis}|E_\nu, E_\mu^{reco})$

Given by neutrino flux modeling

Muon kinematics measurement

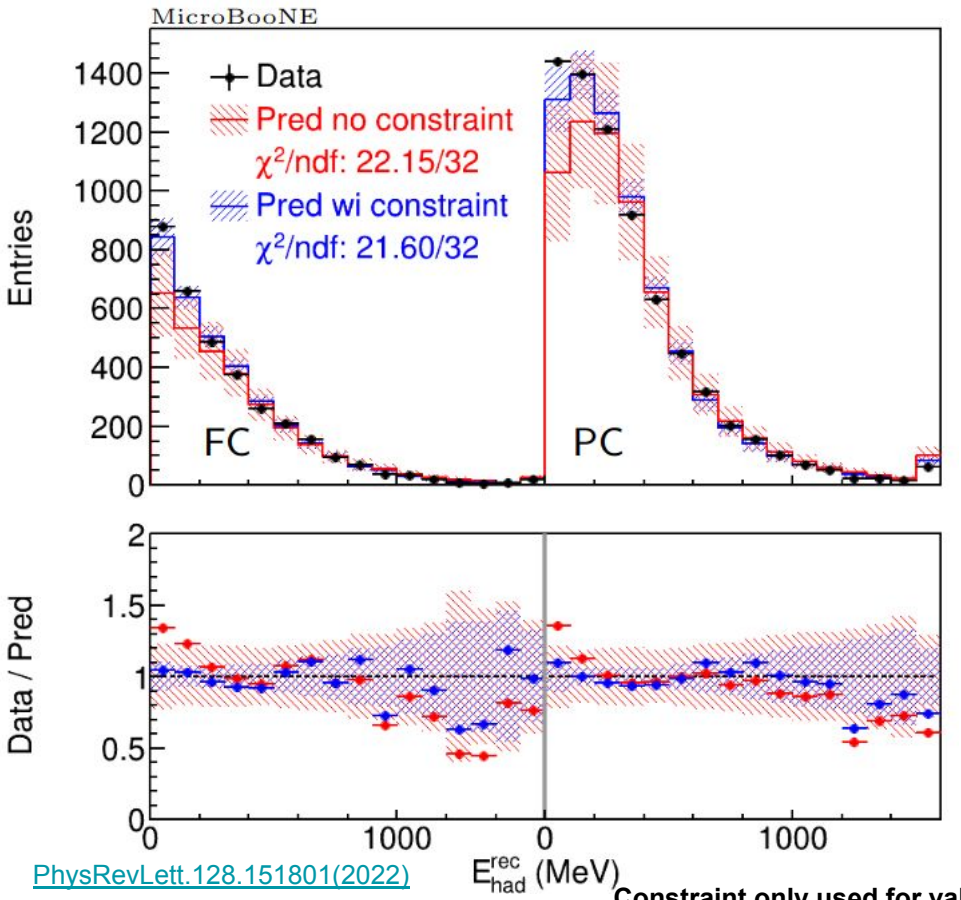

- New method to validate the modeling of neutrino energy
  - Uses LArTPC measurements of lepton kinematics and hadronic energy
- Data/MC goodness of fit tested with χ^2/ndf
  - Muon kinematics used to constrain model prediction of hadronic energy under conditional constraint formalism
- Reduced systematic uncertainties in constrained prediction
- Constraint only used in validation, not unfolding

PhysRevLett.128.151801(2022)

Constraint only used for validation, not unfolding

Model Validation: $M(E_{had}^{vis})$ vs $\mu(E_{had}^{vis}|E_\nu, E_\mu^{reco})$

Given by neutrino flux modeling

Muon kinematics measurement

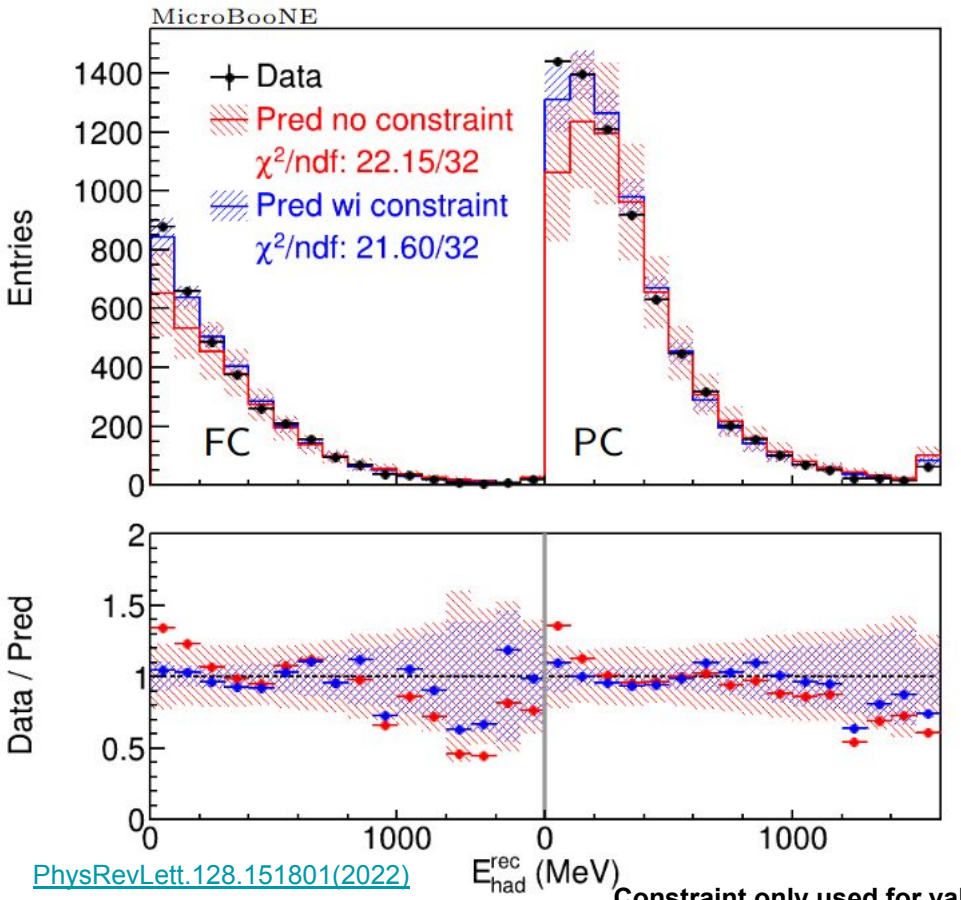

Sensitive to modeling of missing hadronic energy through conservation of energy:

$$E_\nu = E_\mu + E_{had}^{vis} + E_{had}^{missing}$$

- E_μ and E_{had}^{vis} measured directly
- Constrained flux modeling → constrained E_ν prediction

PhysRevLett.128.151801(2022)

Constraint only used for validation, not unfolding

Model Validation of Missing Hadronic Energy

- Conditional constraint procedure akin to reweighting based on P_μ measurement
- QE, RES, MEC, DIS predict different P_μ, $E_{had}^{missing}$ and E_{had}^{vis} distributions
  - The constrained prediction of E_{had}^{vis} is sensitive to the modeling of $E_{had}^{missing}$ in each process
- Measurement of constrained E_{had}^{vis} is thus sensitive to the model processes used in $E_{had}^{missing}$ → validation of **the mapping between true and reconstructed E_ν**

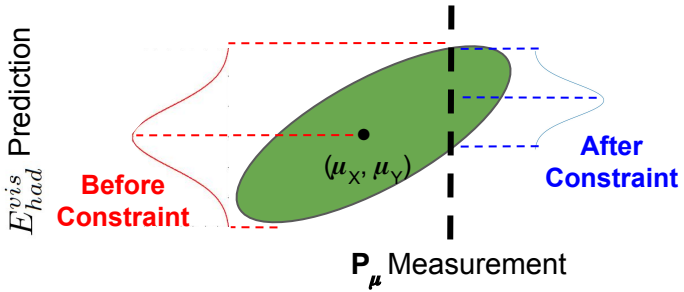

For Illustrative Purposes Only:

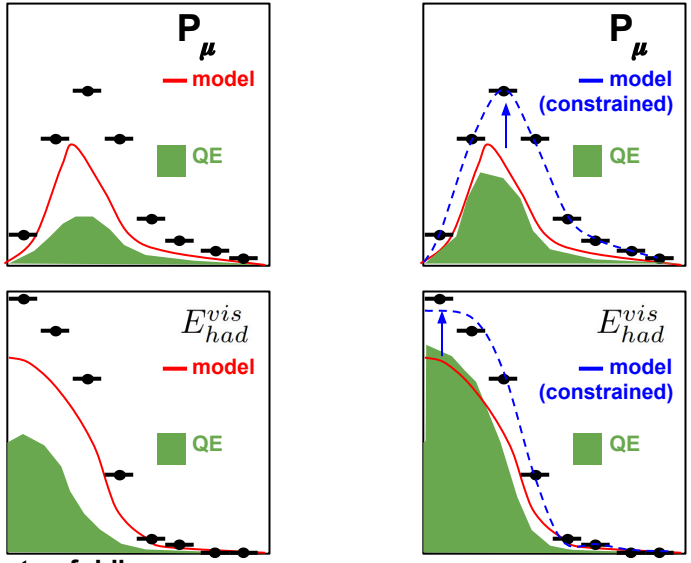

Constraint only used for validation, not unfolding

Testing Model Validation Procedure with Fake Data

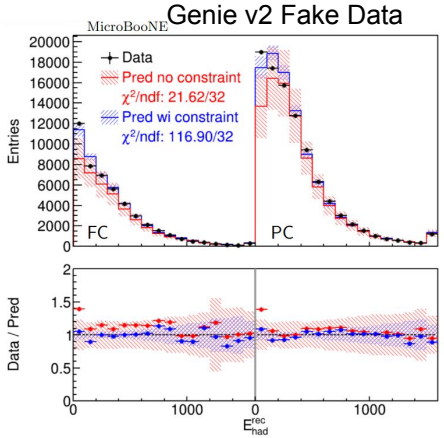

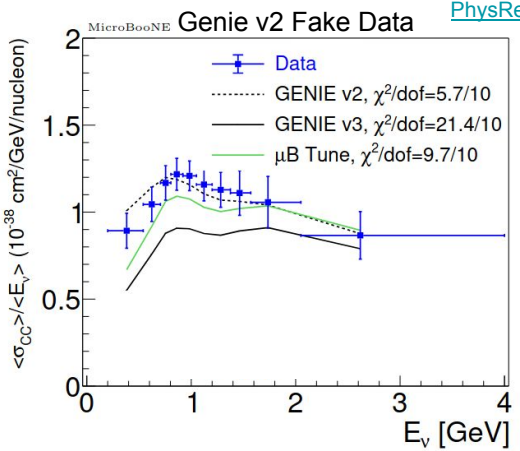

PhysRevLett.128.151801(2022)

Fake Data	Model Validation GoF χ^2/ndf (p-value)	Unfolded XS w.r.t truth χ^2/ndf (p-value)
Genie v2	116.9/32 (1e-10)	5.7/10 (.84)
-30% E_p	47.1/16 (6.6e-5)	5.2/10 (.88)

Constraint only used for validation, not unfolding

- Don't unfold real data if it fails model validation
- Fake data generated from scratch with Genie v2 prediction
  - Additional fake data study taking uBooNE prediction and reducing proton energy
- Constrained model prediction fails validation test→ $E_{had}^{missing}$ modeling disagreement
- Unfolded XS consistent with truth
  - Xs extraction is less sensitive to data/model discrepancy than the model validation

Model Validation in Multiple Dimensions w. Real Data

Muon Energy Distribution

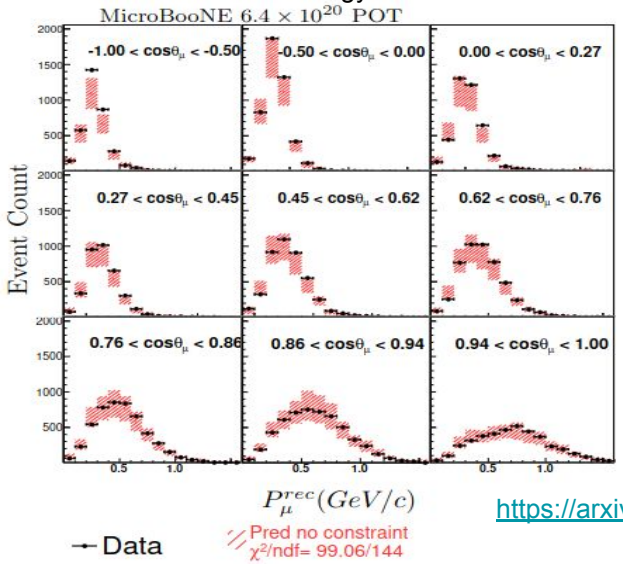

Hadronic Energy Distribution

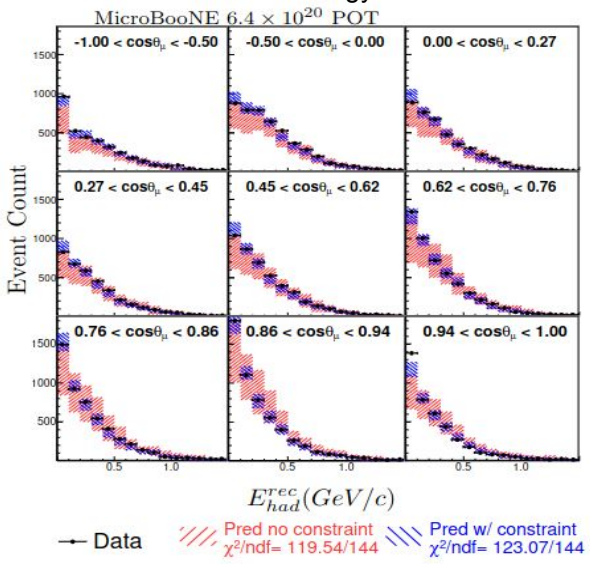

https://arxiv.org/abs/2307.06413

- 2D distribution w/ constraint covers 3D phase space
- Real data passes validation test in 1D and 2D
- Model uncertainty is sufficient to cover potential bias introduced in unfolding

9 angle slices in $\cos(\theta_\mu)$:
{-1, -0.5, 0, 0.27, 0.45, 0.62, 0.76, 0.86, 0.94, 1}
1-6 P_μ bins within each angle slice

Constraint only used for validation, not unfolding

Wiener SVD Unfolding and Regularization

- **Nominal flux-averaged XS** unfolded with Wiener SVD method (JINST 12 P10002)
  - Maximizes the overall signal to noise ratio through the application of the Wiener filter

$$M_i = \Sigma_j R_{ij} \cdot S_j + B_i$$

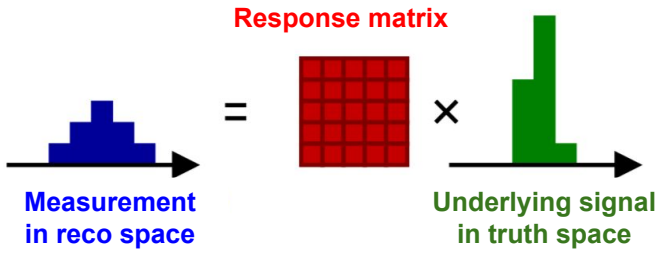

- Reported covariance matrix includes all statistical and systematic **(previously validated) model** uncertainties

- Bias introduced in regularization and unfolding captured in a **(known) smearing matrix A_C**

- **Ingredients** to perform a fair comparison between reported Xs and event generator predictions

Regularized using derivatives computed along each of E_ν, P_μ, $\cos(\theta_\mu)$, combined in quadrature:

$$T^2_{reg} = T^2_{reg,E\nu} + T^2_{reg,P\mu} + T^2_{reg,\cos(\theta)}$$

*No conditional constraint used in unfolding

Previous Single-Differential Energy-Dependent XS

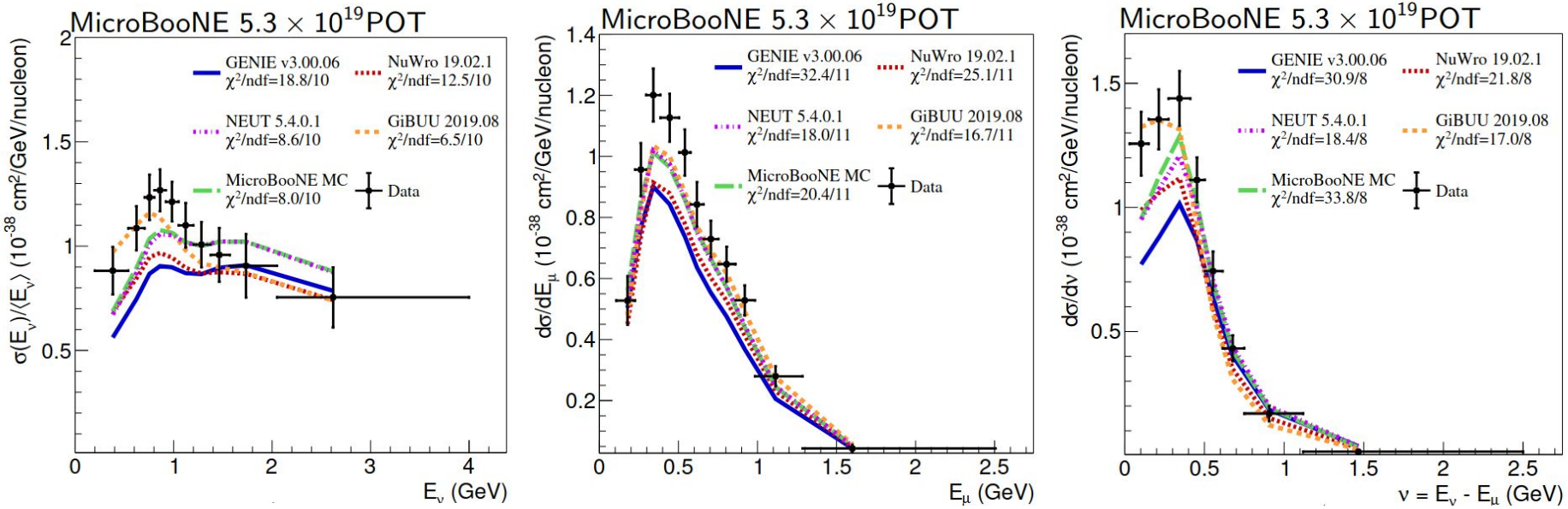

PRL 128, 151801 (2022)

Used 5x10^{19} POT data

Energy-dependent Xs measurements enabled by the new model validation procedure for $E_\nu^{reco} \rightarrow E_\nu^{true}$ mapping

Unfolded Measurement in 3D

https://arxiv.org/abs/2307.06413

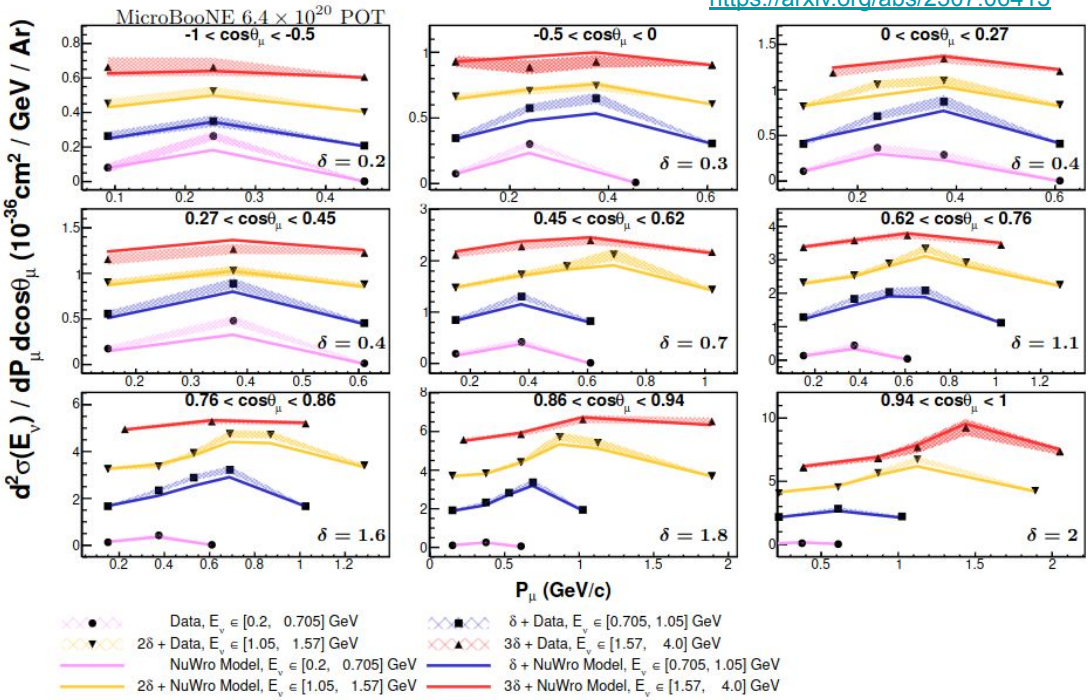

Data plotted against NuWro prediction

E_ν slices overplot with offset N*δ for each angle slice

δ in same units of $d^2\sigma$

$(E_\nu)/dP_\mu dcos(\theta_\mu)(10^{-36}cm^2/GeV/Ar)$

Unfolded Measurement in 3D

https://arxiv.org/abs/2307.06413

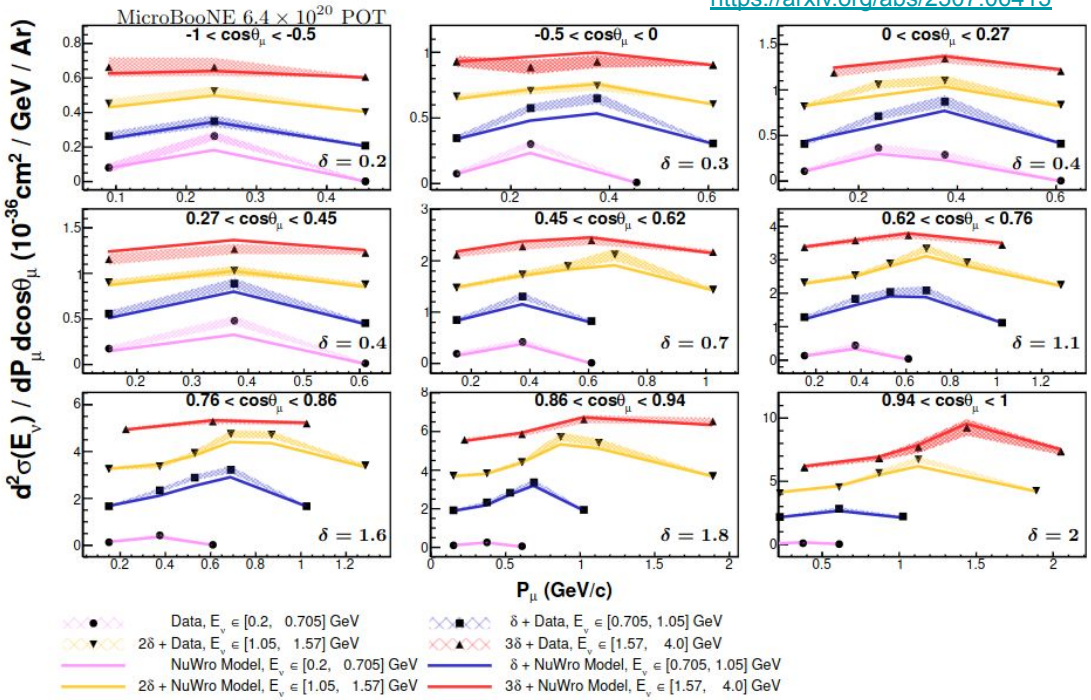

Data plotted against NuWro prediction
E_ν slices overplot with offset N*δ for each angle slice
δ in same units of $d^2\sigma$
$(E_\nu)/dP_\mu dcos(\theta_\mu)(10^{-36}cm^2/GeV/Ar)$

Model Generator	χ^2/ndf
Genie v2.12.10	741.1/138
Genie v3.0.6 (MicroBooNE Tune)	326.1/138
Genie v3.0.6 (Untuned)	322.2/138
GIBUU 2021	269.9/138
NEUT v5.4.0.1	243.3/138
NuWro v19.02.01	212.1/138

Descending χ^2/ndf →

3D measurement contains wealth of information → all model central value predictions are now in tension with data

More powerful than 1D measurement, which was consistent with some models

Example of Usage: Integrated muon momentum for 2D XS

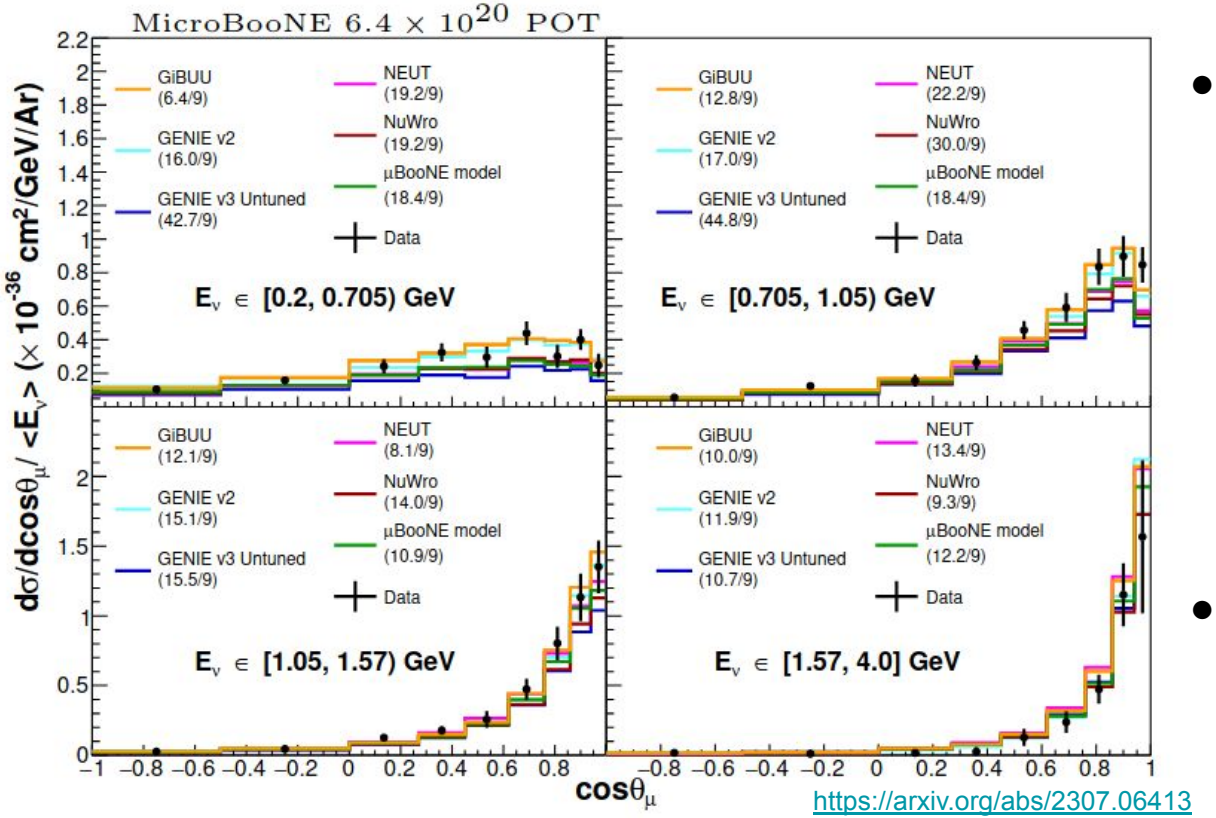

https://arxiv.org/abs/2307.06413

- Model performances vary over E_ν
  - **GiBUU** performs the best at low energy
  - **MicroBooNE tune** performs much better than **Genie v3 (untuned)** at low energies, corresponding to energy region of T2K data used in the tune
  - **NuWro** gives best prediction at high E_ν, forward angle, where RES fraction is higher
- ν-interaction channels vary over energy range
  - QE fraction 75%→55% from lowest to highest E_ν bin

Low Energy: E_ν in [0.2, 0.705) GeV

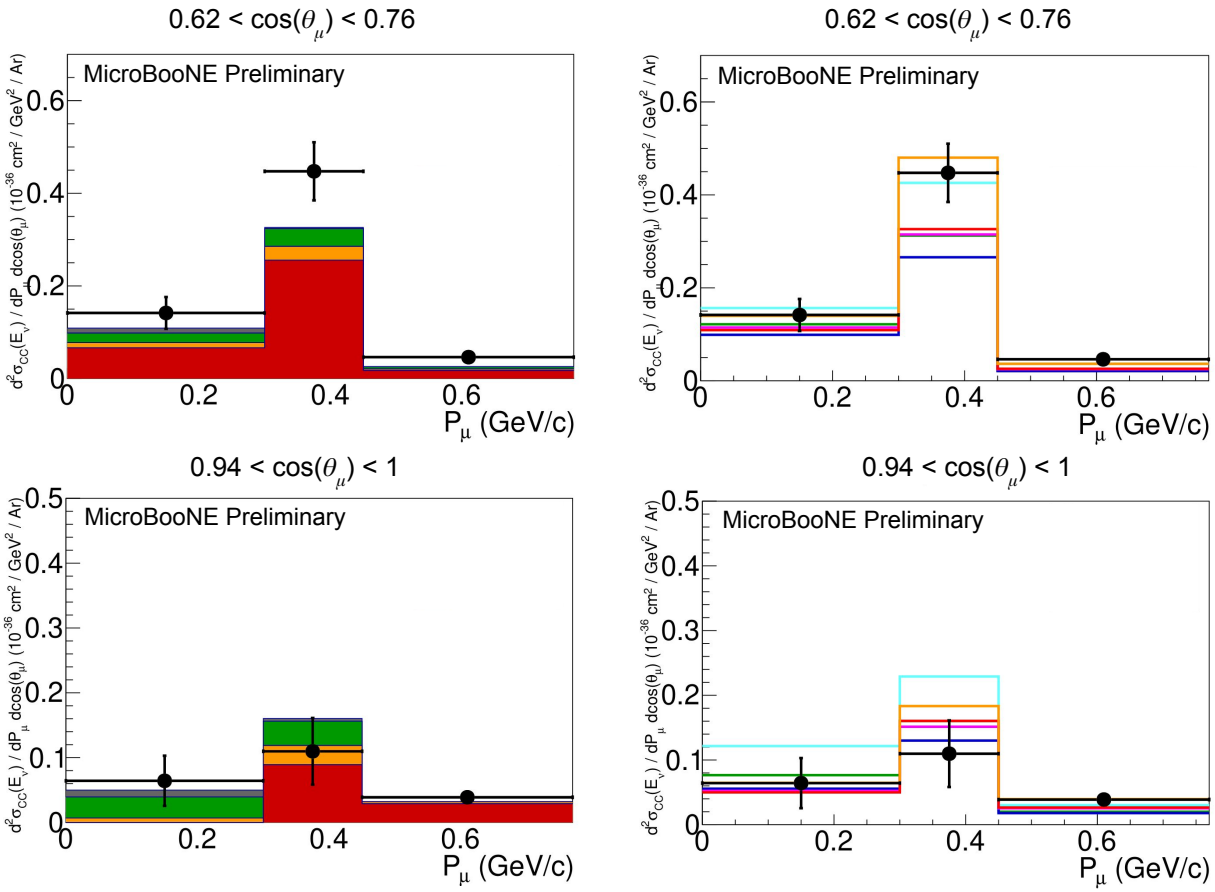

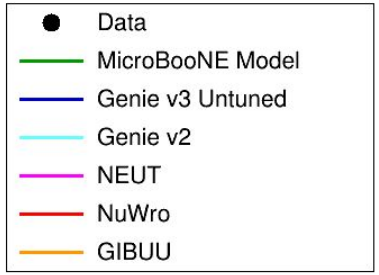

- **GIBUU** performance best in this energy region with χ^2 of 6.4/9
- Other models consistently under-predict XS at P_μ peak
- Data deficit seen at extreme forward angle

Single Pion includes all non-DIS sources

High Energy: E_ν in [1.57, 4.0] GeV

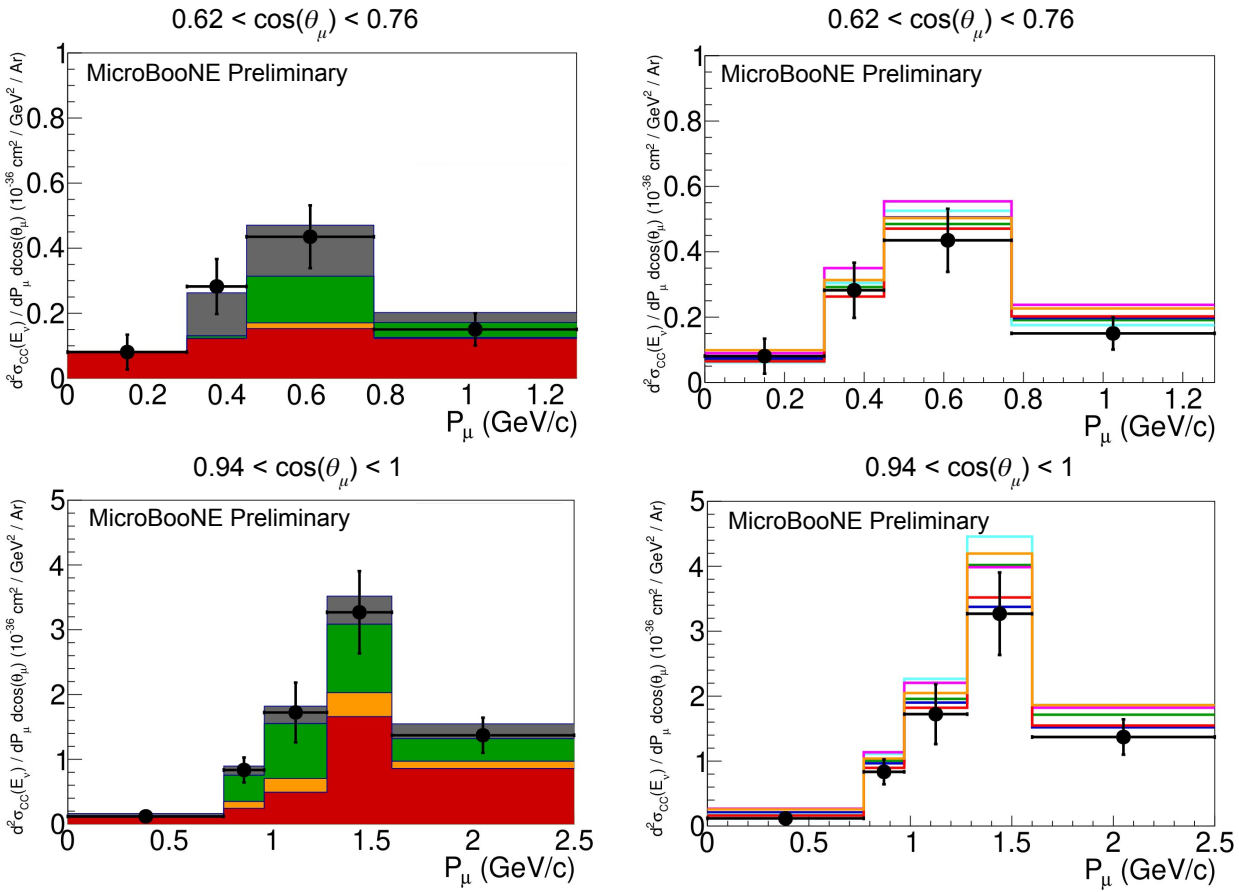

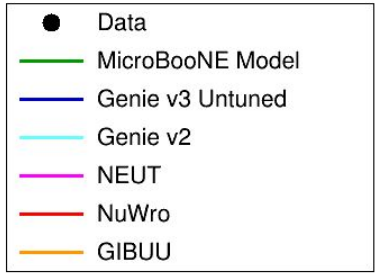

- **NuWro** performs well at high energies, particularly at forward angles
  - This is a region of high pion production
- All models consistently over-predict XS at P_μ peak, less disagreement on tails

Single Pion includes all non-DIS sources

Outlook

- Many exciting results in the works at MicroBooNE
  - Twice as much MicroBooNE data available
  - NuMI+BNB combined measurement for improved flux uncertainty
  - Follow-up analysis investigating hadronic final state: 0 protons vs N protons
  - Analyses on electron neutrinos, proton multiplicity, pion production, NuMI beam measurements, rare searches, methodology, …

- Future accelerator neutrino experiments will determine mass ordering and CP violation
  - This measurement can aid neutrino interaction modeling at DUNE

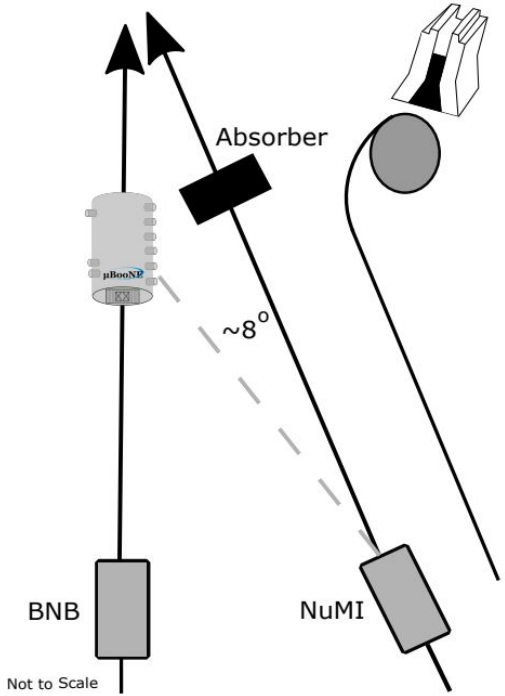

Summary

Triple-differential cross sections for inclusive ν_μ CC are measured with high precision in MicroBooNE with LArTPC technology

- 3D phase space spans inclusive ν_μ CC interaction channel
- Cross section as a function of E_ν are hugely important to oscillation experiments and model development
- New model validation procedure with conditional covariance allows for a validation of mapping to E_ν
- This measurement aids model development for DUNE and SBN program

https://arxiv.org/abs/2307.06413

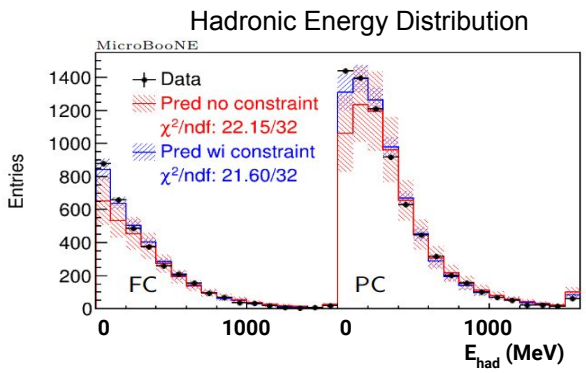

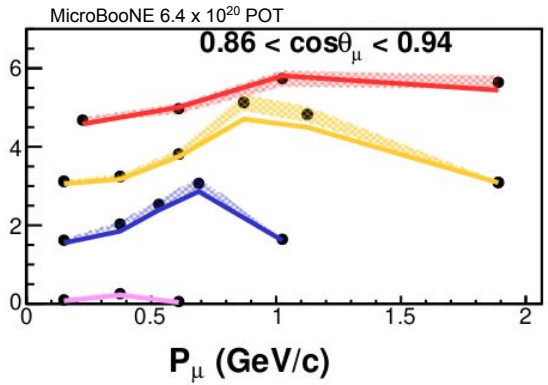

Thank You!

Backup

nuPRISM

- nuPRISM: a technique to obtain effective mono-energetic neutrino flux with a series of off-axis beams
  - An in-situ calibration with the same beamline for FD
  - A direct calibration of the energy modeling with mono-energetic beam
- Practical constraints likely require neutrino cross section models

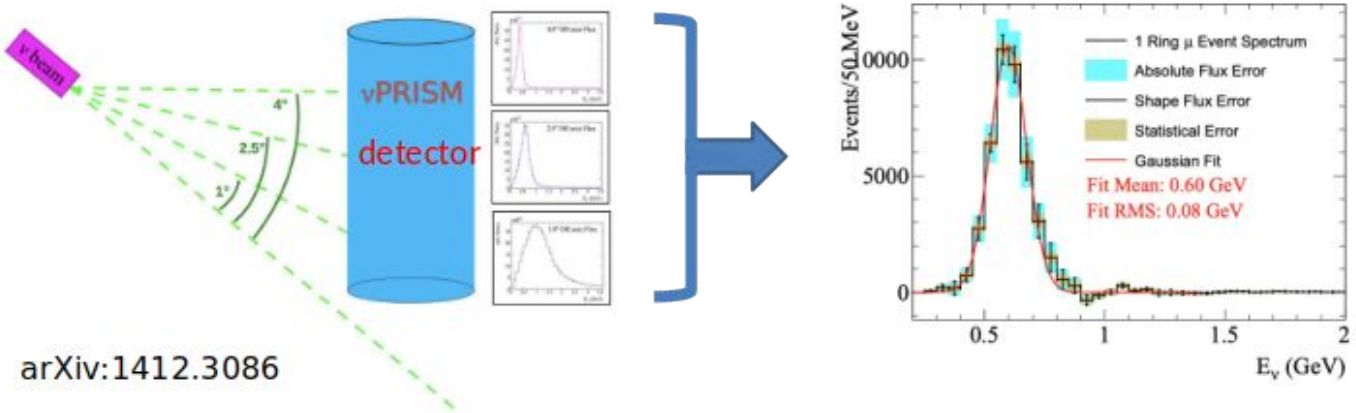

arXiv:1412.3086

Difficulties from (broadband) beam

- The precision of measurement is limited by large beam flux uncertainty
- Broadband beam flux no mono-energetic beam to calibrate detector response

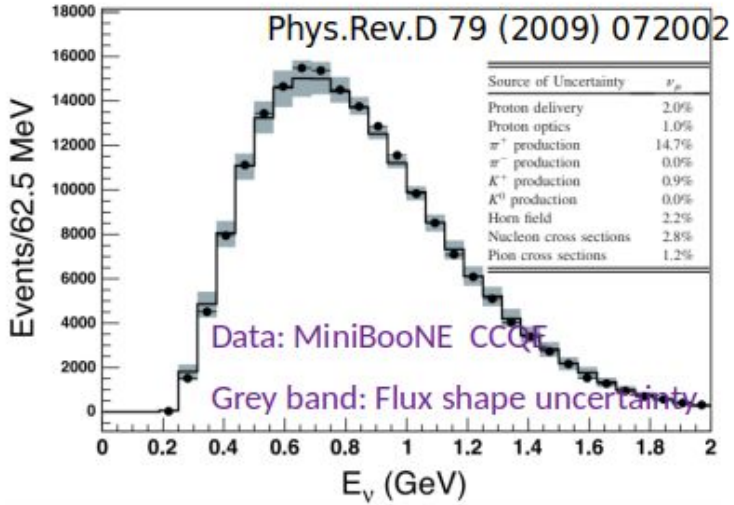

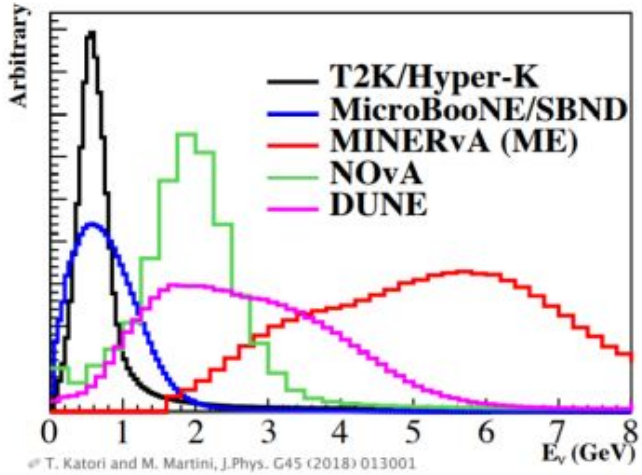

Searching for LEE

- ν_e analyses
  - restricting to quasi-elastic kinematics (Deep Learning , 1e1p)
  - MiniBooNE-like final state (Pandora, 1eNp0π, 1e0p0π)
  - all ν_e final states (Wire-Cell, 1eX)
- single photon analysis
  - targeting Delta radiative decay hypothesis (Pandora, 1γ1p, 1γ0p)

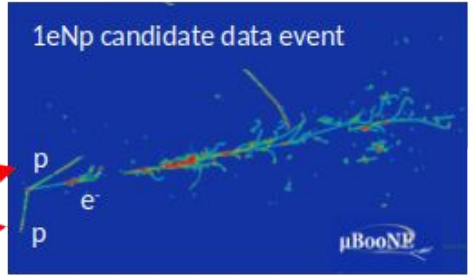

- 4 analyses, 6 final states

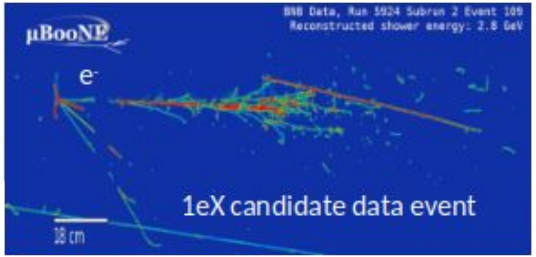

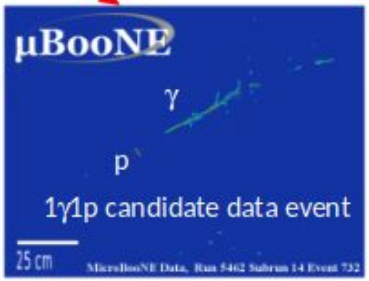

Search for Low-Energy Excess in ν_eCC

Channels	Reconstruction	Efficiency	Purity	Data Events
CCQE 1e1p	Deep Learning	6.6%	75%	25
1e0p0π	Pandora	9%	43%	34
1eNp0π	Pandora	15%	80%	64
Inclusive 1eX	Wire-Cell	46%	82%	606

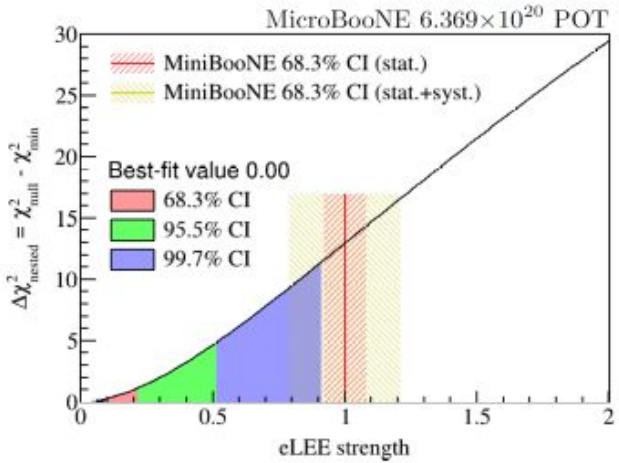

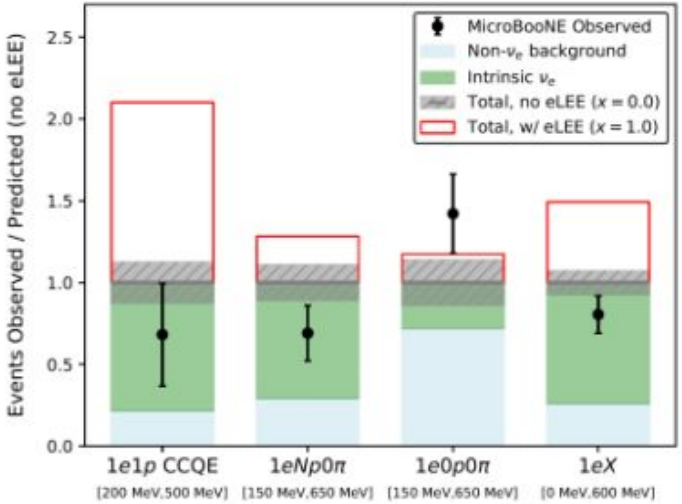

arXiv:2110.14054

ν_e cannot be the sole explanation of MiniBooNE excess!

Signal Processing

- Goal: convert raw wire current to charge measurement
- Naive solution: 1D deconvolution
  - Uses Fourier transform and average wire response to deconvolve
  - Struggles with certain “topologies” such as prolonged tracks
- Improvement: 2D deconvolution
  - Solve all wires simultaneously, removing charge position ambiguity
  - Reduced noise through Wiener filter
  - More robust result, now imported to all 3 MicroBooNE reconstruction chains

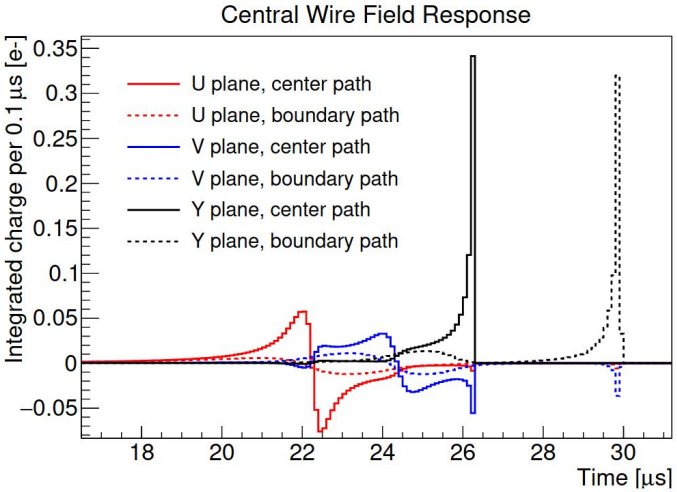

JINST 13 P07006

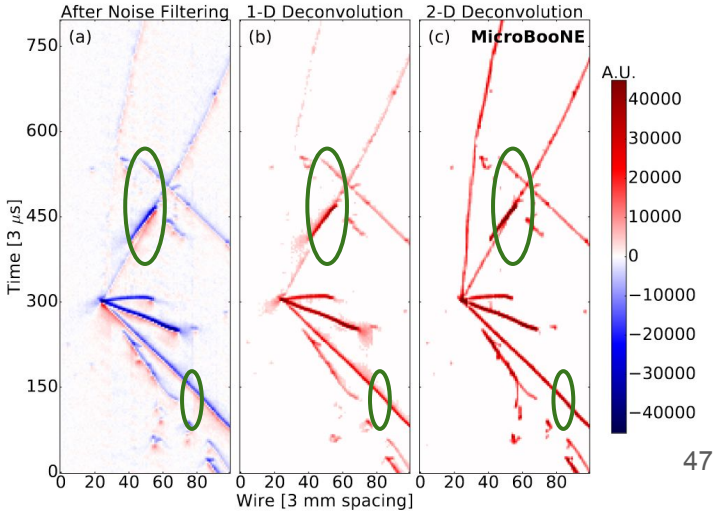

MicroBooNE Dead Wires

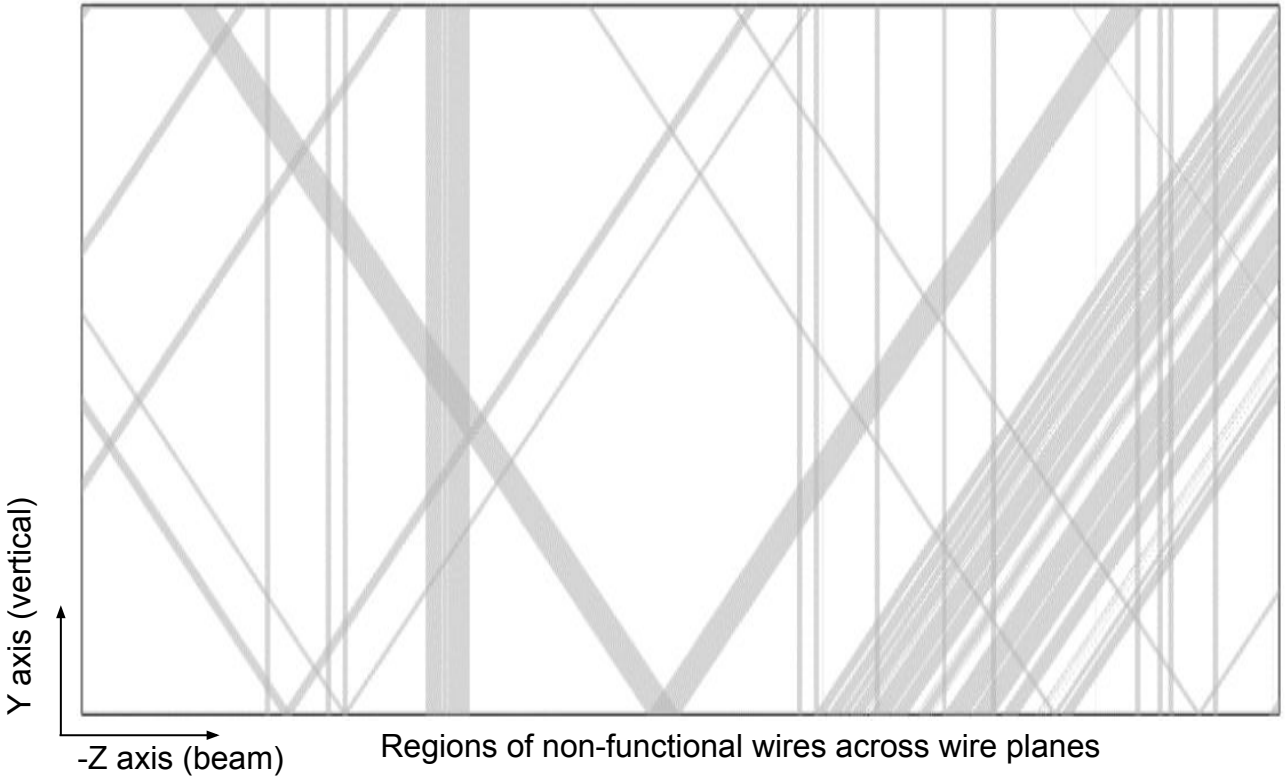

Regions of non-functional wires across wire planes

JINST 16 P06043

Imaging and Clustering

- Principle of tomographic imaging: 2D projections -> 3D image
  - Widely used, such as in medicine (CT scan)
  - Only have 3 projections
  - Under-determined system y=Ax:
    ~3n wires (y) but ~n^2 intersections (x)

- Compressed sensing used to solve ambiguity
  - Leverages intuition of sparsity
  - Minimizes number of reconstructed hits
  - L1 norm is used, allowing gradient descent to solve

- Connected hits are clustered into 3D point cloud

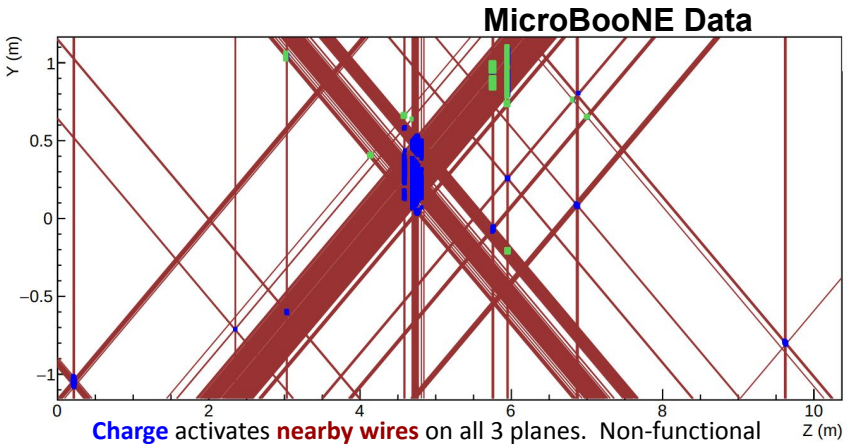

Charge activates **nearby wires** on all 3 planes. Non-functional wires and 2-plane requirement lead to **ghost hits** (later removed).

JINST 16 P06043

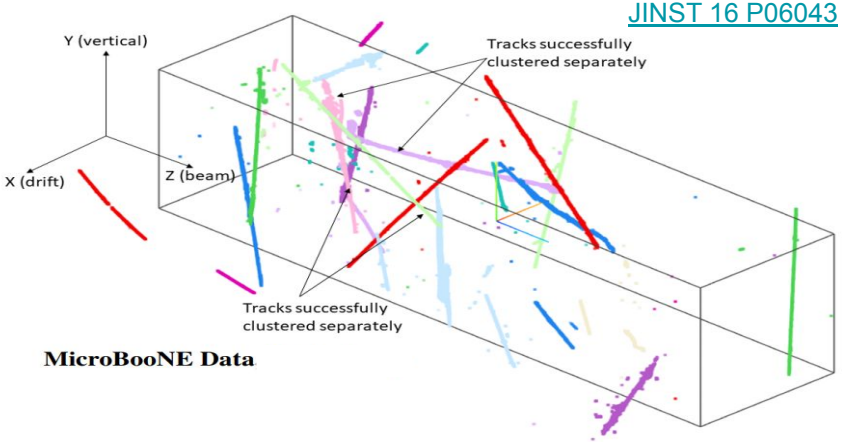

Charge is grouped into clusters representing different particle interactions.

Imaging and Clustering

Principle of tomographic imaging:
2D projections -> 3D image

- Widely used, such as in medicine (CT scan)
- Proximity of hits in space and time used to form clusters and remove artificial **ghost hits**
- Combines charge information across wire planes for **good energy resolution**
- Wire plane redundancy combats dead wire issue, keeps detector **fully active**
- Precisely reconstructed 3D charge distribution enables **good angle resolution** later in reconstruction

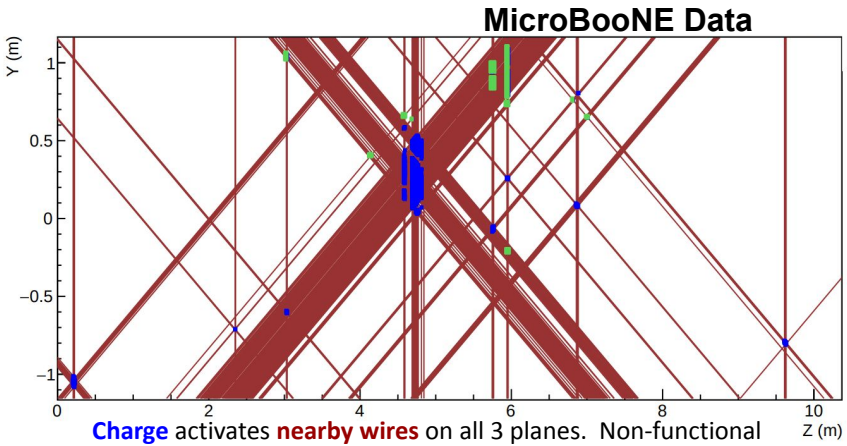

Charge activates **nearby wires** on all 3 planes. Non-functional wires and 2-plane requirement lead to **ghost hits** (later removed).

JINST 16 P06043

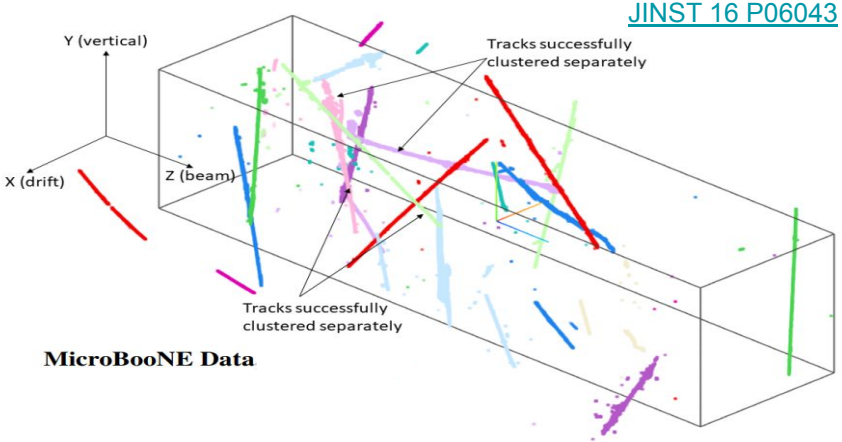

Charge is grouped into clusters representing different particle interactions.

Charge-Light Matching

- 2,300 μs readout window but only 1.6 μs beam window
  - Light info is prompt, timing at ~ns level
  - Charge-light matching connects light info to charge cluster

- Simple solution: only match BNB-coincident flash(es)

- Many-to-many matching: attempt to match every flash and cluster
  - Simultaneous fit: minimize χ^2 test statistic of measured vs predicted flash
  - Bonus: matching cosmic rays generates large dataset for mapping detector boundary

MicroBooNE Data JINST 16 P06043

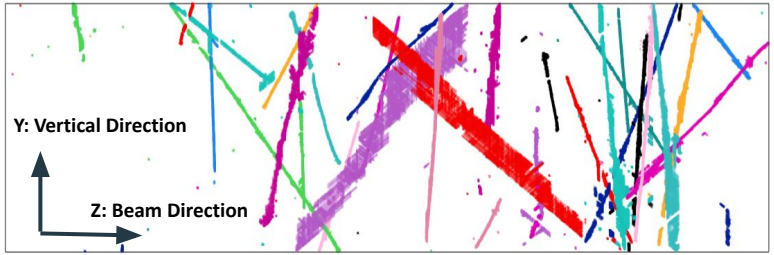

Top: a drift window with ~20 cosmic rays

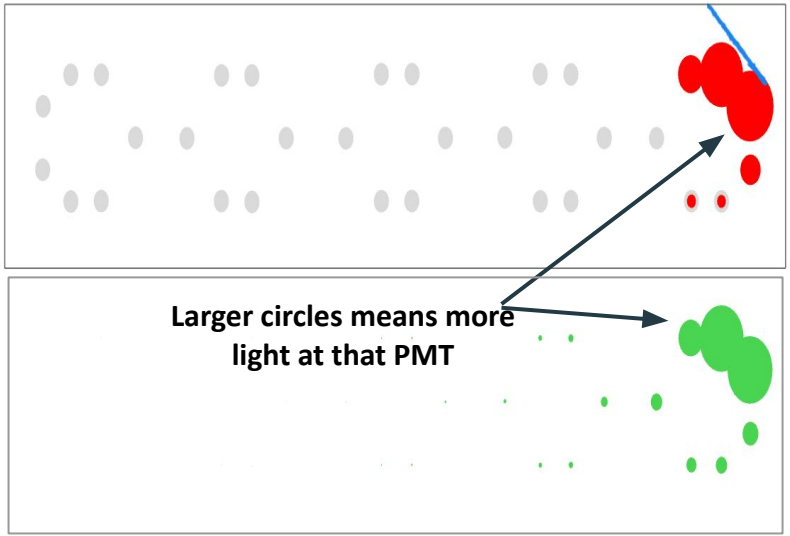

Bottom: The observed (upper) and predicted (lower) light patterns for a single cosmic ray.

Trajectory Fitting

- Allows determination of particle ID and kinematics
- Point cloud of charge organised into graph
  - Shortest path across graph used as trajectory seed
  - Steiner tree forces path to include high-charge areas
- Trajectory fit by minimizing chi2, then dQ/dx is fit
- Trajectories are iteratively fit, one particle at a time

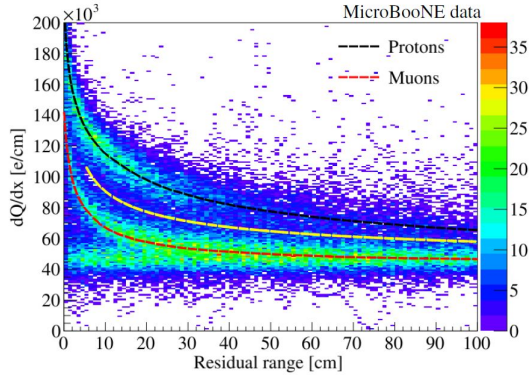

Separation of dQ/dx curves between protons and muons. PhysRevApplied.15.064071

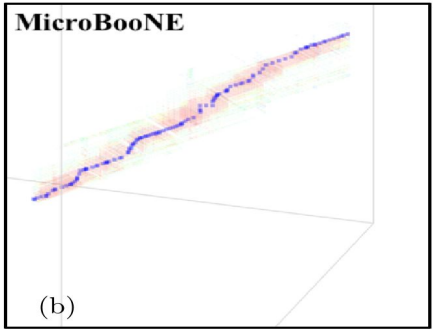

Example of **trajectory fit** through a **point cloud of charge**.

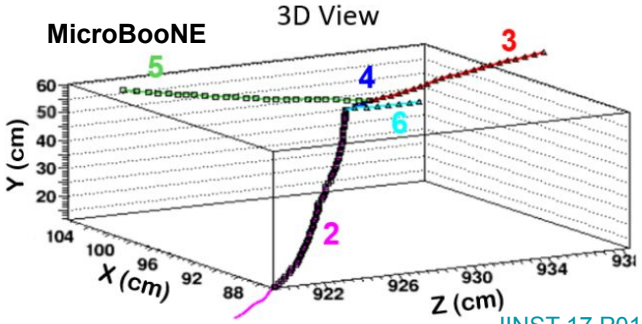

JINST 17 P01037

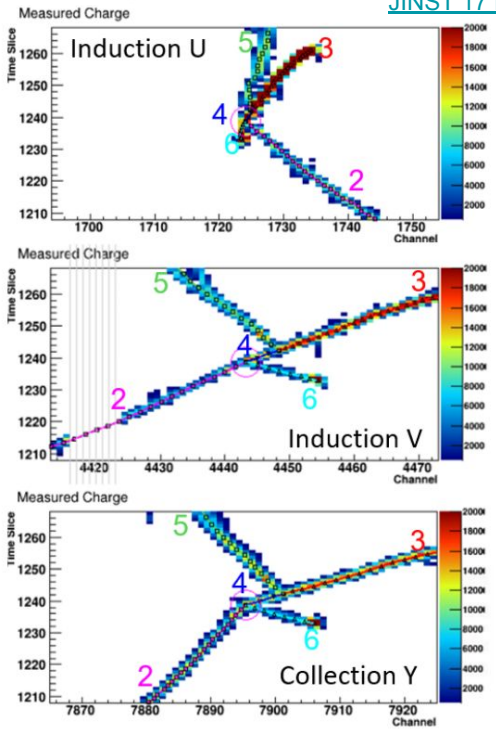

Cosmic Ray Tagging

Throughgoing Muons

Two detector-boundary intersections required

Enabled by many-to-many matching

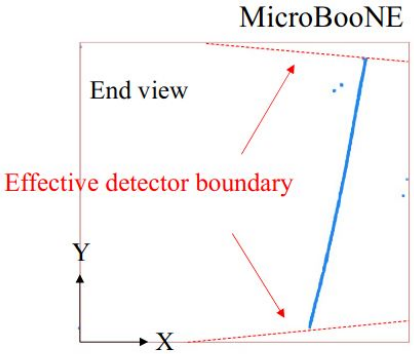

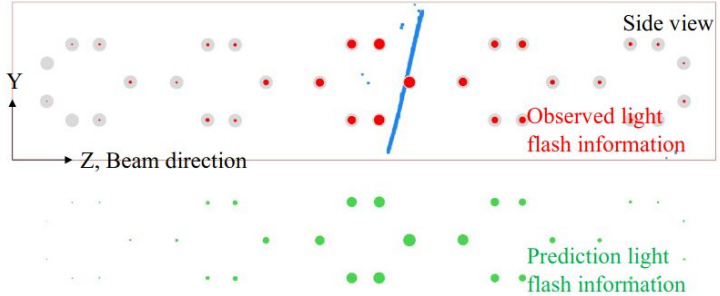

Stopped Muons

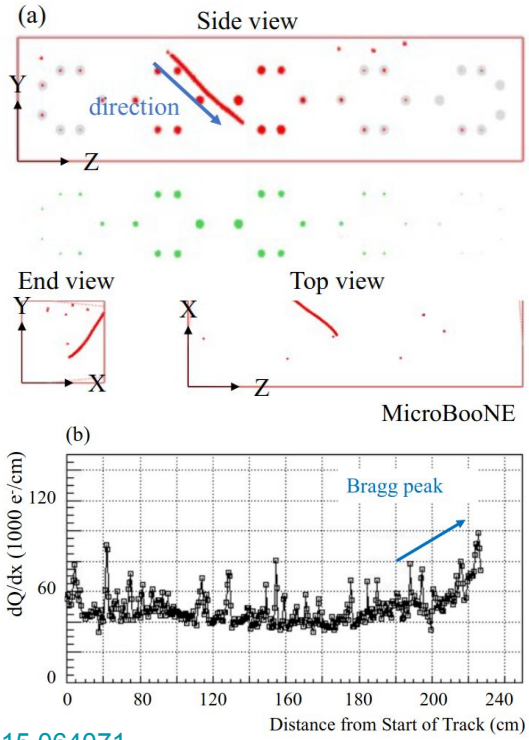

Single boundary intersection required

Particle direction determined from dQ/dx

Only exiting particles are removed

PhysRevApplied.15.064071

Generic Neutrino Detection

- Hardware trigger: BNB drift window
- Software trigger: Light activity required
- Charge-light matching: remove non-beam-coincident cosmic rays
- Dedicated taggers achieve further ~30x reduction
- Roughly 80% efficiency and purity

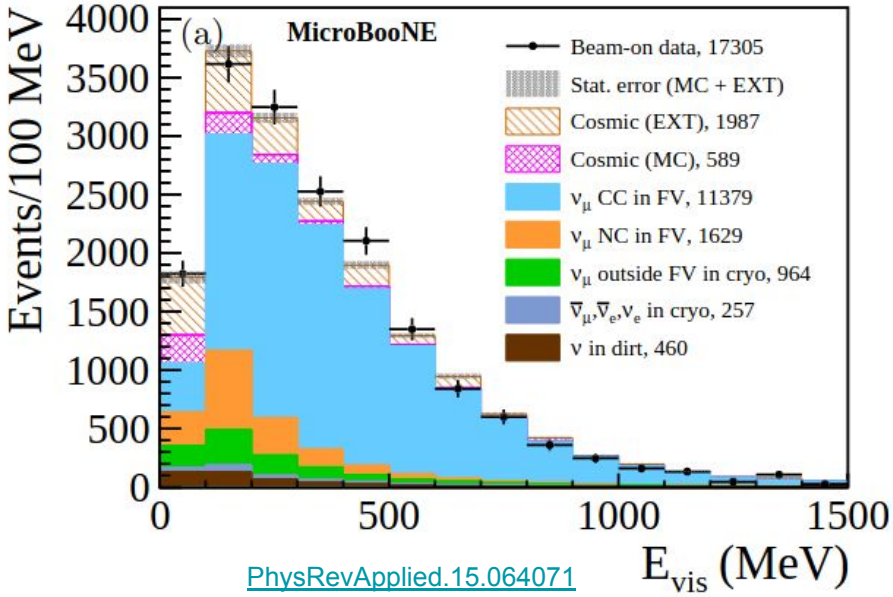

PhysRevApplied.15.064071

Selection Cut	ν_μCC Efficiency	Background Reduction	ν : Background
Hardware Trigger	100%	1(1)	1 : 20,000
Software Trigger	$(98.31 \pm 0.03)\%$	$(0.998 \pm 0.002) \times 10^{-2}(0.01)$	1 : 210
Charge-Light Matching	$(92.1 \pm 0.01)\%$	$(2.62 \pm 0.04) \times 10^{-4}(0.026)$	1 : 6.4
TGM Rejection	$(88.8 \pm 0.01)\%$	$(4.4 \pm 0.2) \times 10^{-5}(0.17)$	1.1 : 1
STM Rejection	$(82.9 \pm 0.01)\%$	$(1.4 \pm 0.1) \times 10^{-5}(0.32)$	2.8 : 1
LMM Rejection	$(80.4 \pm 0.01)\%$	$(6.9 \pm 0.6) \times 10^{-6}(0.50)$	5.2 : 1

Breakdown of efficiency and purity at each selection stage.
Relative background reduction given in parentheses.

Pattern Recognition and Particle Flow Diagram

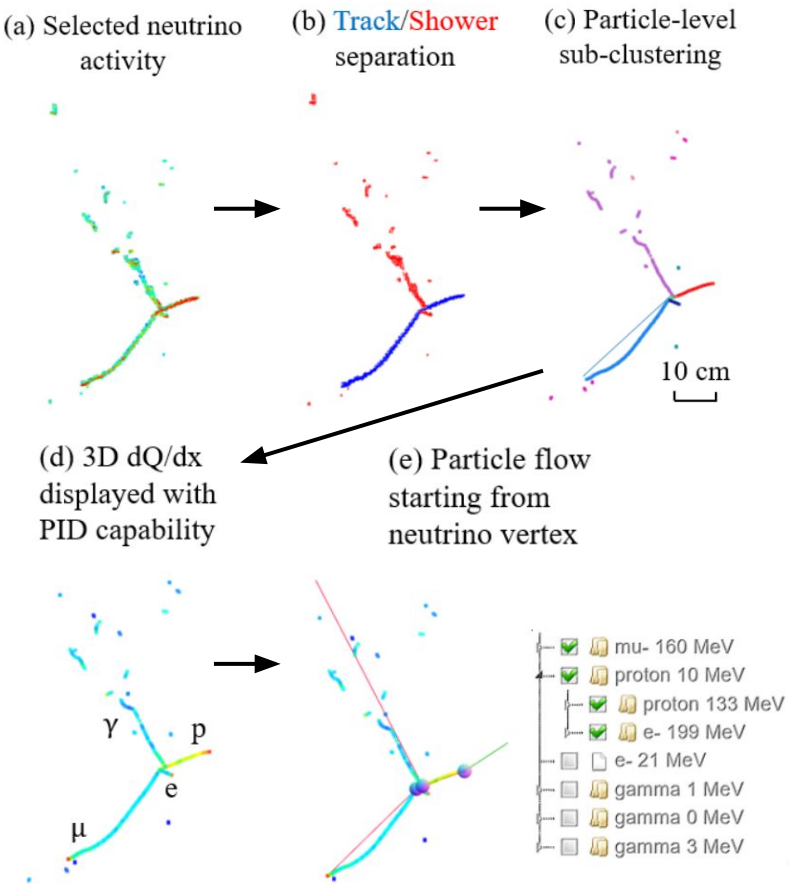

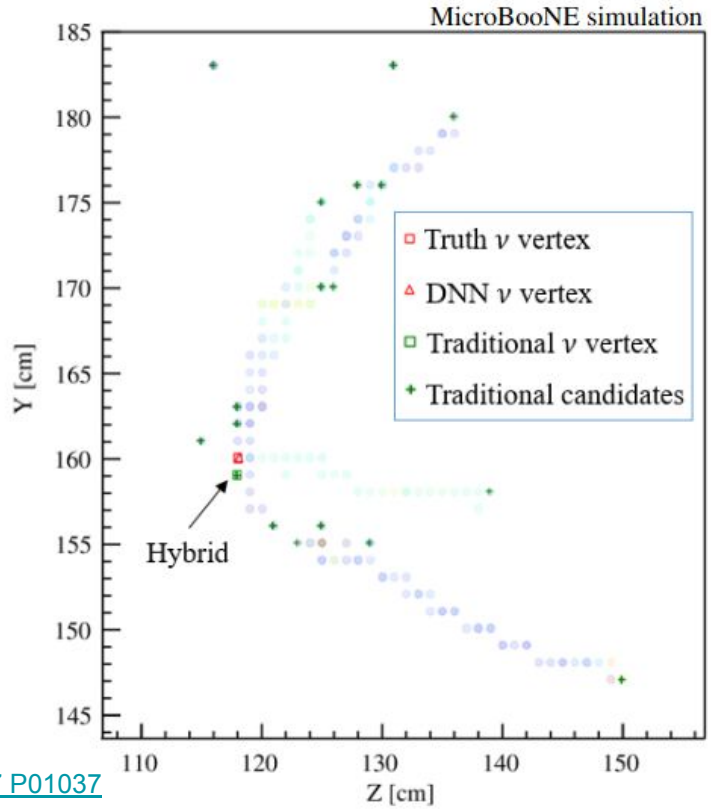

JINST 17 P01037

Neutrino Energy Reconstruction

- Tracks:
  - Residual range is default, summed dE/dx in edge cases
  - Calibrated using stopped muons and protons
- Showers:
  - Scaled charge to account for recombination and bias
  - Calibrated using π^0 invariant mass reconstruction
- $E_\nu = \Sigma E_{particle}$
  - Invariant mass included for muons and pions
  - Binding energy included for protons
- Fully Contained (FC) E_ν resolution: 15-20%

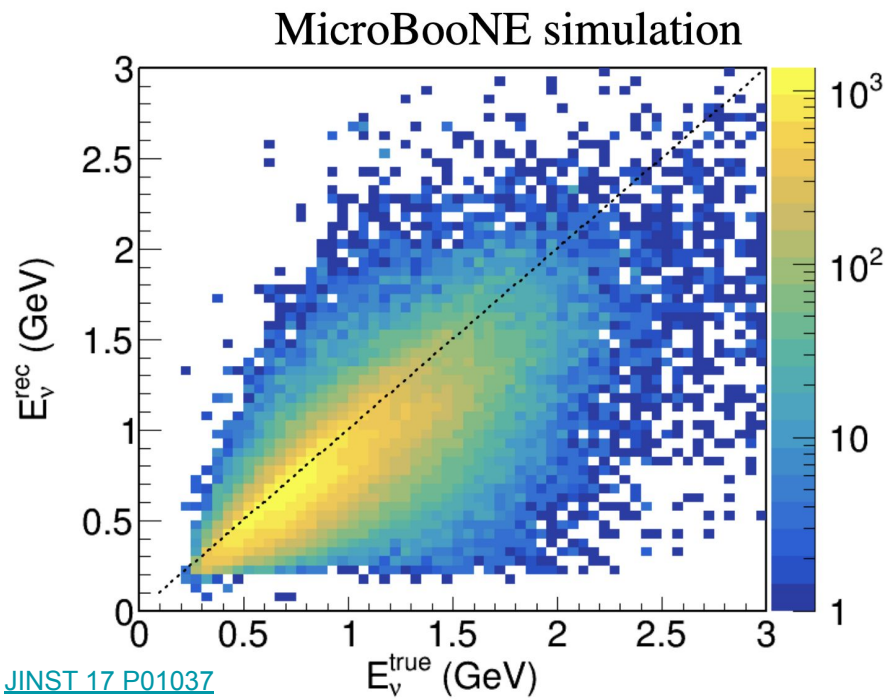

JINST 17 P01037

Neutrino energy resolution for fully contained charged current events

Pi0 Mass Reconstruction

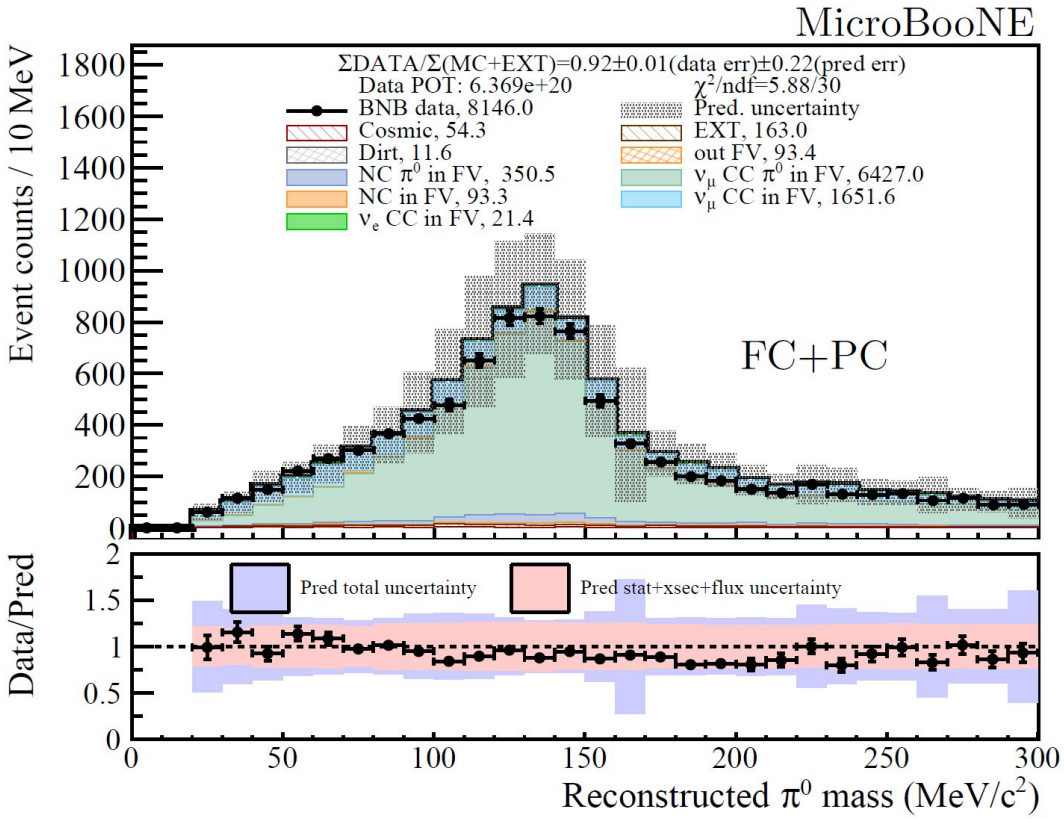

Boosted Decision Tree (BDT) Selection using XGBoost

- Extreme Gradient Boosting:
  - Decision tree complexity controlled through regularization term in loss function
  - Allows for huge number (100+) of features used, resilient to overfitting

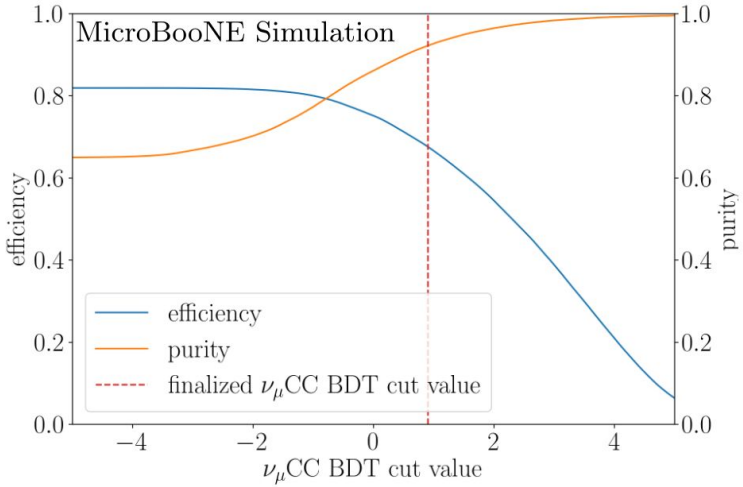

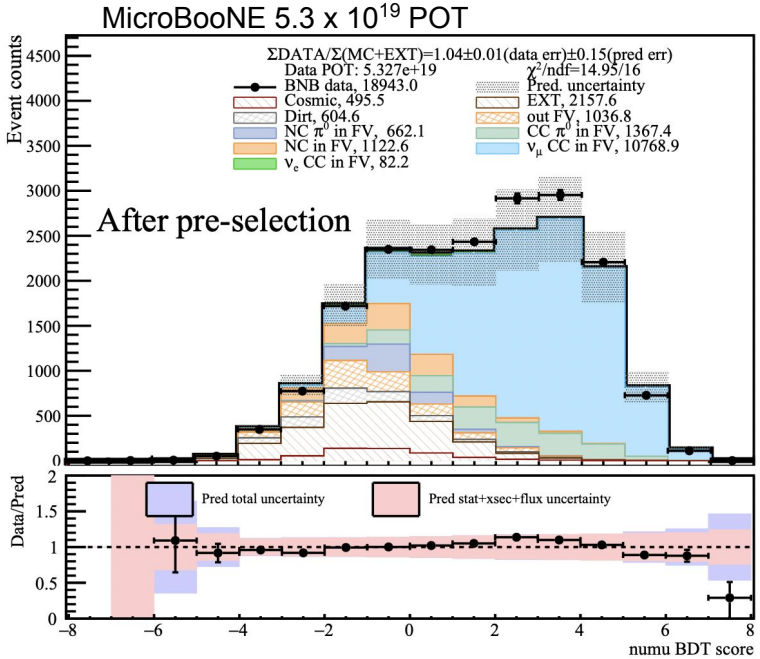

Phys. Rev. D 105, 112005

Note: generic neutrino detection signal includes some ν_μCC backgrounds (ν_e, ν_μNC)

How to estimate systematic uncertainties?

- Full systematic covariance

$$\Sigma^{syst} = \Sigma^{flux} + \Sigma^{xsec} + \Sigma^{det} + \ldots$$

Multisim

Unisim

	Multisim	Unisim
# of parameter variation at a time	Many	One
Parameter(s) variation	Random	Exactly 1
# of MC run	One	Many (one per parameter)
Technical treatment	Event reweighting	Bootstrapping

Flux and cross section systematics: multisim

- Standard reweighting approach, each event has different weights from the randomization of the underlying model parameters.

Tuning parameter name	Parameter type
π^+ hadron production	FLUX
π^- hadron production	FLUX
K^+ hadron production	FLUX
K^- hadron production	FLUX
K^0_L hadron production	FLUX
horn current distribution	FLUX
horn current calibration	FLUX
nucleon total scattering Xs	FLUX
nucleon inelastic scattering Xs	FLUX
nucleon quasi-elastic scattering Xs	FLUX
pion total scattering Xs	FLUX
pion inelastic scattering Xs	FLUX
pion quasi-elastic scattering Xs	FLUX
MicroBooNE GENIE All	GENIE Xs (μB tune)
Strength of the CCQE RPA correction	GENIE Xs (μB tune)
Parameterization of the CCQE nucleon axial form factor	GENIE Xs
Parameterization of the CCQE nucleon vector form factors	GENIE Xs
Changes angular distribution of nucleon cluster in MEC	GENIE Xs (μB tune)
CCMEC Cross-section Shape	GENIE Xs (μB tune)
Angular distribution for RES $\Delta \to N + \pi$	GENIE Xs
Angular distribution for RES $\Delta \to N + \gamma$	GENIE Xs (μB tune)
Scaling factor for CC coherent π production	GENIE Xs (μB tune)
Scaling factor for NC coherent π production	GENIE Xs (μB tune)
Second-class vector current	Xs
Second-class axial current	Xs
π^- interactions	GEANT4
π^+ interactions	GEANT4
proton interactions	GEANT4

Neutrino flux

Neutrino-argon cross section

Final-state hadron-argon interaction

Geant4Reweight: JINST 16 (2021) 08, P08042

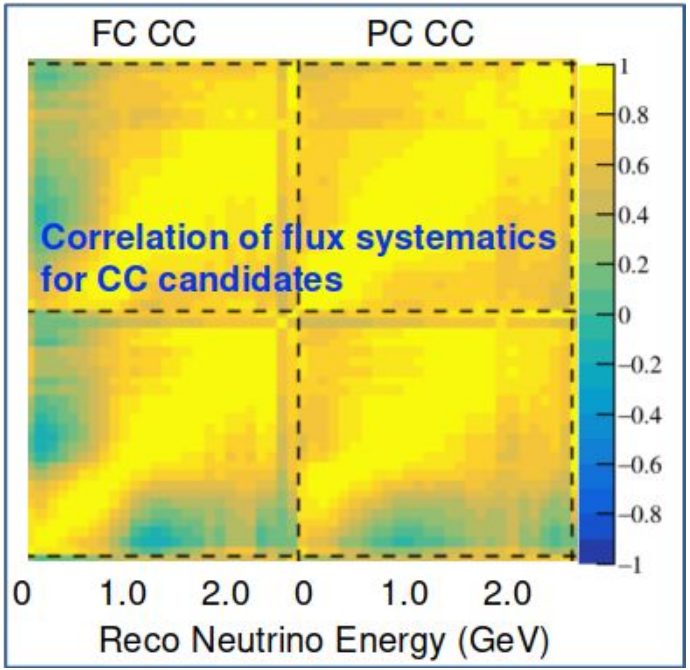

Detector systematics: unisim

- Four major categories
  1) Light yield and propagation
  2) Charge readout detector response
  3) Recombination model (to conversion)
  4) Space charge effect (impacts on E-field)

- For each source of the systematic uncertainty, the same set of MC simulation events are re-simulated with a change to the detector modeling parameter of interest. In total, we have two samples
  1) One sample with nominal value of all parameters: CV sample
  2) One sample with changed value of interested par: 1σ sample

Can not calculate the covariance matrix by the two samples in traditional way, which needs many samples with different pars values:

$$COV_{ij} = EXP\left(\left(X_i - \overline{X}\right)\left(X_j - \overline{X}\right)\right)$$

Detector systematics: bootstrapping method

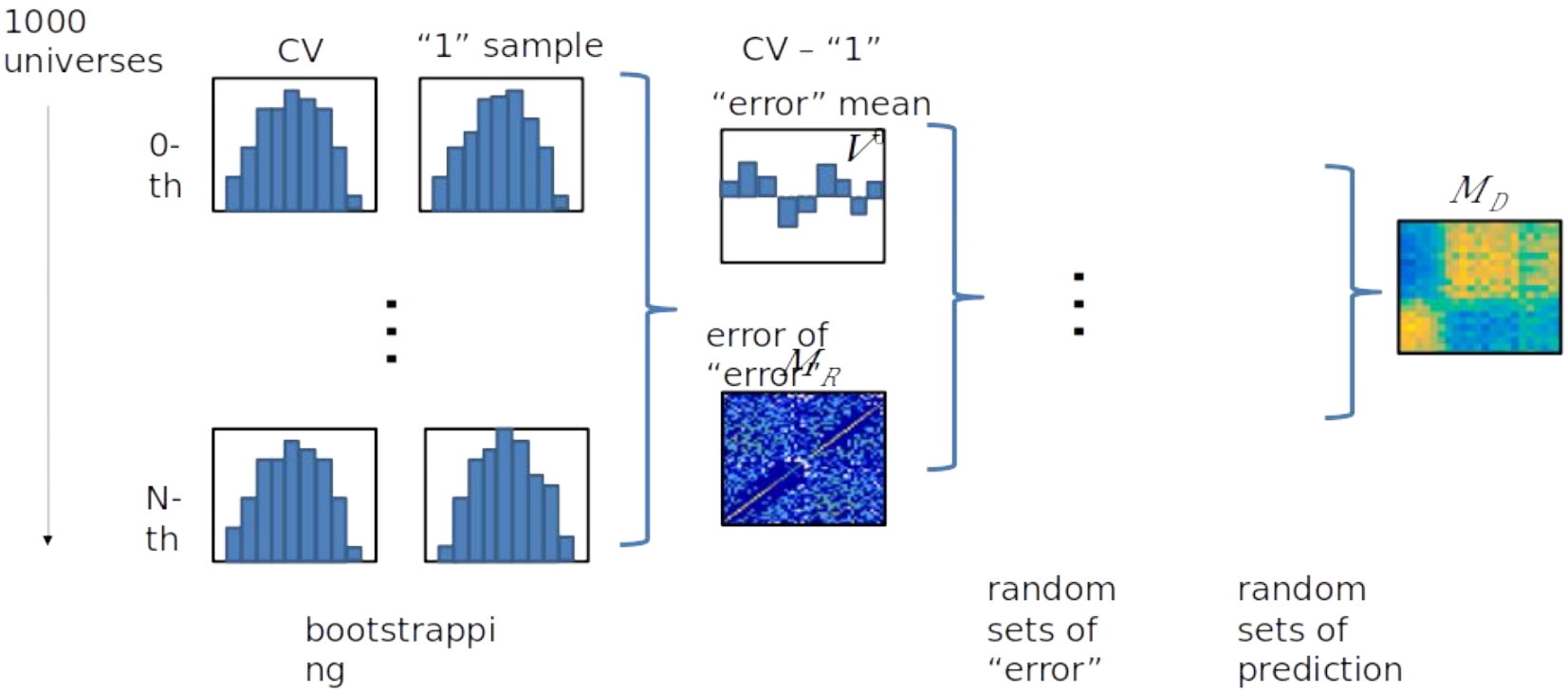

Gaussian Processes Regression

$$\hat{\mu}_{a|b} = \mu_a + \Sigma_{K,ab}\Sigma_{T,bb}^{-1}(x_b - \mu_b)$$

Input bins b

$$\hat{\Sigma}_{T,a|b} = \Sigma_{K,aa} - \Sigma_{K,ab}\Sigma_{T,bb}^{-1}\Sigma_{K,ba}$$

Posterior bins a

$$\Sigma_K(x_1, x_2) = e^{-|(\vec{x}_1 - \vec{x}_2)\cdot\vec{s}|^2/2}$$

Inverse length scales s

Leveraging Cross Section Measurements

- Use of nominal-flux-averaged XS measurement allows for comparison with model prediction
- A non-E_ν-dependent XS measurement can be difficult for theorists to accurately use
  - Measurement must be published with nominal flux prediction and uncertainties
  - Theorist must generate predicted event distribution from nominal flux & uncertainties
  - Not clear how to determine correlations between theorist's prediction (including flux uncertainty) and XS measurement (also including flux uncertainty)
- Enu-dependent XS measurement avoids this issue
  - We handle flux uncertainty in producing the measurement, can be directly compared with prediction
- Extensive model validation is performed to confirm that model bias is within listed uncertainties
- Unfolding reports XS measurement in truth variables for direct comparison
  - Unfolding bias is captured in A_C matrix, reported with measurement, for direct data vs model comparison

Validate

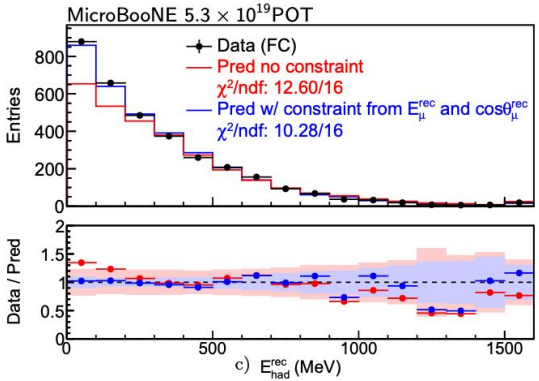

Measure

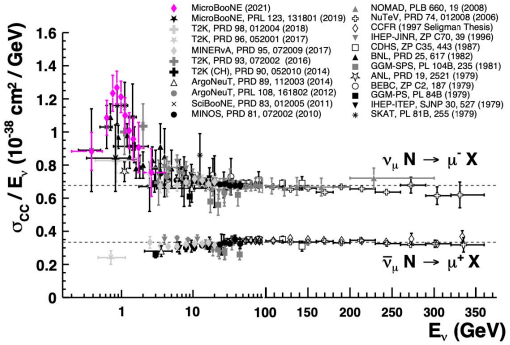

Testing Model Validation Procedure with Fake Data

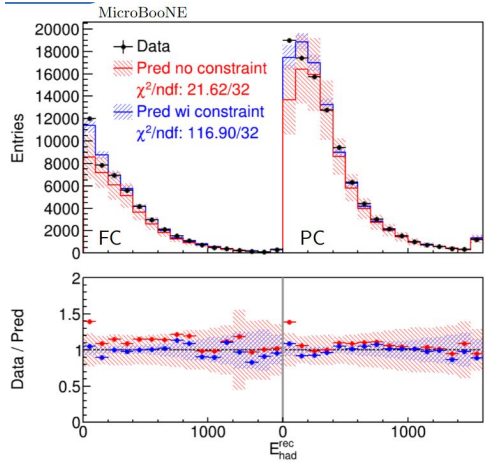

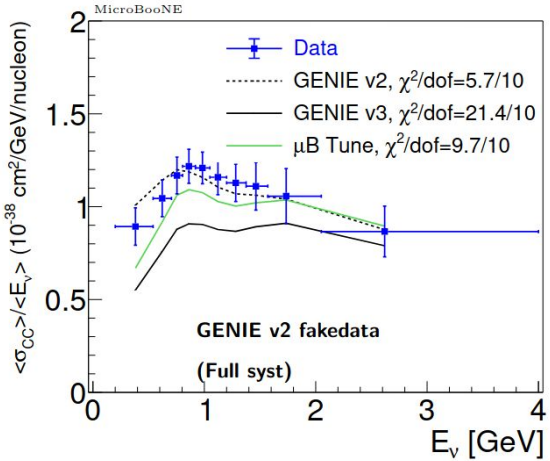

Fake Data	GoF χ^2/ndf	Unfolded XS w.r.t truth χ^2/ndf	Type of Uncertainties Stat. + Syst.
Genie v2	116.9/32	5.7/10	Fluctuations + Full
-15% E_p	39.5/16	4.1/10	Asimov + Xs only
-30% E_p	47.1/16	5.2/10	Asimov + Full

- Fake data generated from scratch with Genie v2 prediction
  - 7.2×10^{20} POT exposure used
- Constrained model prediction fails validation test (**χ^2/ndf = 116.9/32, p-value = 1.3×10^{-11}**) → $E_{had}^{missing}$ modeling disagreement
- Unfolded XS consistent with truth (**χ^2/ndf = 5.7/10, p-value = 0.84** → Xs extraction is less sensitive to data/model discrepancy than the model validation)
  - Consistent with expectation
  - Similar observation in other fake data sets

Model Validation in One Dimension w. Real Data

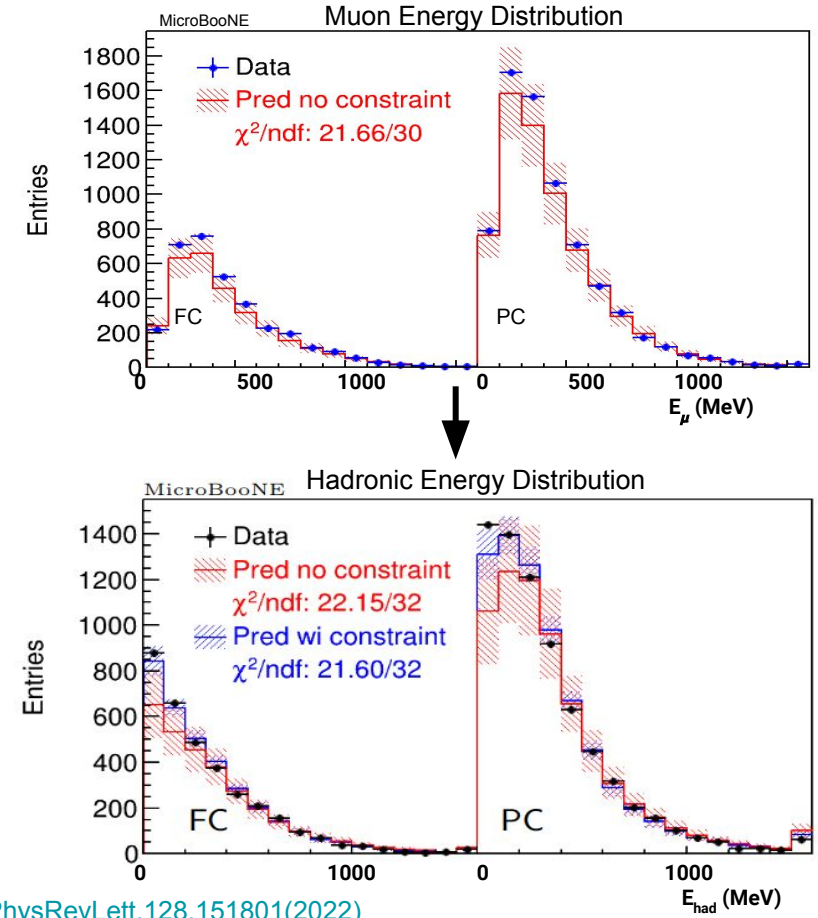

- 2D distribution w/ constraint covers 3D phase space
- Real data passes validation test in 1D and 2D
- Therefore model uncertainty is sufficient to cover potential bias introduced in unfolding

9 angle slices in $\cos(\theta_\mu)$:
{-1, -0.5, 0, 0.27, 0.45, 0.62, 0.76, 0.86, 0.94, 1}
16 P_μ bins within each angle slice

PhysRevLett.128.151801(2022)

Constraint only used for validation, not unfolding

Equation For Unfolding

$$M_i - B_i = \sum_j R_{ij} \cdot S_j$$

$$\Longleftrightarrow$$

$$\boxed{\chi^2 = (\boldsymbol{M} - \boldsymbol{B} - \boldsymbol{R} \cdot \boldsymbol{S})^T \cdot \boldsymbol{V}^{-1} \cdot (\boldsymbol{M} - \boldsymbol{B} - \boldsymbol{R} \cdot \boldsymbol{S})}$$

$$R_{ij} = \tilde{\Delta}_{ij} \cdot \tilde{F}_j$$

$$\tilde{\Delta}_{ij} = \frac{POT \cdot T \cdot \int_j F(E_{\nu j}) \cdot \sigma(E_{\nu j}) \cdot D(E_{\nu j}, E_{rec}) \cdot \varepsilon(E_{\nu j}, E_{rec}) \cdot dE_{\nu j}}{POT \cdot T \cdot \int_j F(E_{\nu j}) \cdot \sigma(E_{\nu j}) \cdot dE_{\nu j}}$$

➡ a MC ratio, less sensitive to Xs uncertainty

$$\tilde{F}_j = POT \cdot T \cdot \int_j \bar{F}(E_{\nu j}) \cdot dE_{\nu j}$$

$$S_j = \frac{\int_j \bar{F}(E_{\nu j}) \cdot \sigma(E_{\nu j}) \cdot dE_{\nu j}}{\int_j \bar{F}(E_{\nu j}) \cdot dE_{\nu j}}$$

Not subject to prior knowledge of the Xs uncertainty

- ***V*** is the covariance matrix encoding:
  - Data statistical uncertainty: **M**
  - Flux uncertainty: **B, R (F)**
  - Cross-section (Xs) uncertainty: **B, R (σ)**
  - GEANT4 hadron interaction uncertainty: **B, R (D, ε)**
  - Detector-model uncertainty: **B, R (D, ε)**
  - "Dirt" uncertainty: **B**
  - POT uncertainty (2%): **M**
  - MC statistical uncertainty: **M**
- The unfolded cross section is defined based on the nominal flux
  - Easy for model comparisons
  - Simple for uncertainty calculation

PRD 102 (2020) 113012

Equation For Unfolding

Measurements

Flux

Cross section

Detector response

Selection efficiency

Background

$$M(E_{rec}) = POT \cdot T \cdot \int F(E_\nu) \cdot \sigma(E_\nu) \cdot D(E_\nu \to E_{rec}) \cdot \varepsilon(E_\nu, E_{rec}) \cdot dE_\nu + B(E_{rec})$$

$$M_i = \sum_j R_{ij} \cdot S_j + B_i$$

$$R_{ij} = \tilde{\Delta}_{ij} \cdot \tilde{F}_j$$

$$\tilde{\Delta}_{ij} = \frac{POT \cdot T \cdot \int_j F(E_{\nu j}) \cdot \sigma(E_{\nu j}) \cdot D(E_{\nu j}, E_{rec\,i}) \cdot \varepsilon(E_{\nu j}, E_{rec\,i}) \cdot dE_{\nu j}}{POT \cdot T \cdot \int_j F(E_{\nu j}) \cdot \sigma(E_{\nu j}) \cdot dE_{\nu j}}$$

➡ a MC ratio, less sensitive to Xs uncertainty

$$\tilde{F}_j = POT \cdot T \cdot \int_j \bar{F}(E_{\nu j}) \cdot dE_{\nu j}$$

$$S_j = \frac{\int_j \bar{F}(E_{\nu j}) \cdot \sigma(E_{\nu j}) \cdot dE_{\nu j}}{\int_j \bar{F}(E_{\nu j}) \cdot dE_{\nu j}}$$

Not subject to prior knowledge of the Xs uncertainty

Benefit Of the Definition

- Define the flux-averaged cross section using the nominal flux , thus can be easily compared with any model prediction based on the nominal flux

$$S_j = \frac{\int_j \overline{F}(E_{\nu j}) \cdot \sigma(E_{\nu j}) \cdot dE_{\nu j}}{\int_j \overline{F}(E_{\nu j}) \cdot dE_{\nu j}}$$

- Simplify the uncertainty calculation
  - Switch *to F* would bring up complicated systematic correlation
  - Proper treatment of flux shape uncertainty: PRD **102** 113012

$$M_i - B_i = \sum_j R_{ij} \cdot S_j \quad \Longleftrightarrow \quad \chi^2 = (\boldsymbol{M} - \boldsymbol{B} - \boldsymbol{R} \cdot \boldsymbol{S})^T \cdot \boldsymbol{V}^{-1} \cdot (\boldsymbol{M} - \boldsymbol{B} - \boldsymbol{R} \cdot \boldsymbol{S})$$

V is the covariance matrix encoding:

- Data statistical uncertainty: **M**
- Flux uncertainty: **B, R (F)**
- Cross-section (Xs) uncertainty: **B, R (*σ*)**
- GEANT4 hadron interaction uncertainty: **B, R (D, ε)**
- Detector-model uncertainty: **B, R (D, ε)**
- "Dirt" uncertainty: **B**
- POT uncertainty (2%): **M**
- MC statistical uncertainty: **M**

	GENIE 3.0.6	NEUT 5.4.0.1	NuWro 19.2.1	GiBUU 2019.08
Nuclear Model	LFG	LFG	LFG	LFG
QE	Valencia	Nieves	Lwlyn-Smith	standard
MEC	Valencia	Nieves	Nieves	empirical
Resonant	KLN-BS	Berger-Sehgal	Adler-Rarita-Schwinger	MAID (Spin-dependent)
Coherent	Berger-Sehgal	Rein-Sehgal	Berger-Sehgal	
FSI	hA2018 cascade	cascade	cascade	BUU transport model

Inclusive CC measurements

Experiment	Target	References	Efficiency (%)	Purity (%)
ArgoNeuT	Ar	Phys. Rev. Lett. 108 161802 Phys. Rev. D 89 112003	49.5 42.0 (59.0)	95 95.2 (91.2)
MicroBooNE	Ar	Phys. Rev. Lett. 123 131801 Phys. Rev. Lett. **128**, 151801	57.2 68	50.4 92
MINERvA	CH, C/CH, Fe/CH, Pb/CH	Phys. Rev. Lett. 112, 231801 Phys. Rev. D94, 112007 Phys. Rev. Lett. 116	24 ~ 50	60 ~ 80
MINOS	Fe	Phys. Rev. D81, 072002		
NOMAD	C	Phys. Lett. B660, 19	40.9 ~ 73.3	99.3
SciBooNE	CH	Phys. Rev. D83, 12005	34.5	~90
T2K	CH, H_2O, Fe	Phys. Rev. D87, 092003 Phys. Rev. D90, 052010 Phys. Rev. D93, 072002	~50 41.2 ~50 @1GeV	~86 89.4 ~97

TABLE I. Comparisons between various models and the unfolded triple-differential measurement within each E_ν slice.

Model Name	Total χ^2/ndf	[0.2, 0.705] GeV χ^2/ndf	[0.705, 1.05] GeV χ^2/ndf	[1.05, 1.57] GeV χ^2/ndf	[1.57, 4.0] GeV χ^2/ndf
GENIE v2	741.1/138	71.4/28	64.4/35	64.3/42	35.6/33
MicroBooNE model	326.1/138	85.0/28	77.8/35	44.6/42	31.9/33
GENIE v3 untuned	322.2/138	94.1/28	84.8/35	52.2/42	37.3/33
GiBUU	269.9/138	33.8/28	54.8/35	52.6/42	31.0/33
NEUT	243.3/138	58.5/28	59.9/35	43.1/42	38.2/33
NuWro	212.1/138	54.8/28	67.3/35	40.9/42	29.6/33

TABLE II. Comparisons between various models and the unfolded triple-differential measurement within each E_ν slice after integrating over the P_μ dimension.

Model Name	Total χ^2/ndf	[0.2, 0.705] GeV χ^2/ndf	[0.705, 1.05] GeV χ^2/ndf	[1.05, 1.57] GeV χ^2/ndf	[1.57, 4.0] GeV χ^2/ndf
GENIE v2	93.1/36	16.0/9	17.0/9	15.1/9	11.9/9
MicroBooNE model	74.0/36	18.4/9	23.5/9	10.9/9	12.2/9
GENIE v3 untuned	95.3/36	42.7/9	44.8/9	15.5/9	10.7/9
GiBUU	60.6/36	6.4/9	12.8/9	12.1/9	10.0/9
NEUT	66.0/36	19.2/9	22.2/9	8.1/9	13.4/9
NuWro	62.4/36	19.2/9	30.0/9	14.0/9	9.3/9

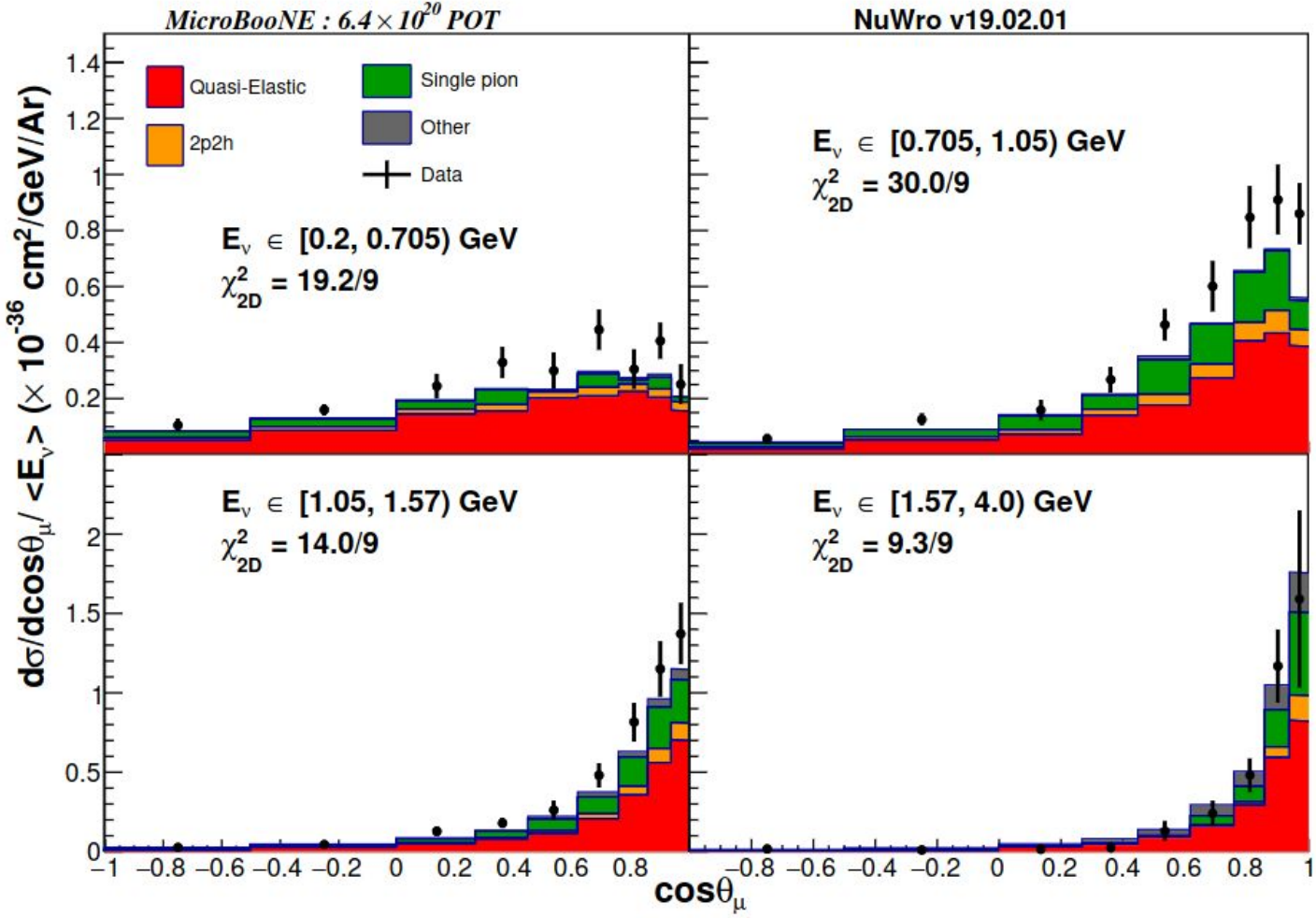
MicroBooNE : 6.4 × 10^20 POT
NuWro v19.02.01
Quasi-Elastic
2p2h
Single pion
Other
Data
E_ν ∈ [0.2, 0.705) GeV
χ²_2D = 19.2/9
E_ν ∈ [0.705, 1.05) GeV
χ²_2D = 30.0/9
E_ν ∈ [1.05, 1.57) GeV
χ²_2D = 14.0/9
E_ν ∈ [1.57, 4.0) GeV
χ²_2D = 9.3/9
dσ/dcosθ_μ / <E_ν> (× 10^-36 cm²/GeV/Ar)
cosθ_μ